Pulsatile Flow of Nanofluids Between Concentric Cylinders

Naeem Ur Rehman
Regn.#278257

This thesis is submitted as a partial fulfillment of the requirements for the degree of
Master of Science
in
Mathematics

Supervised by: Dr. Asim Aziz

Department of Mathematics
School of Natural Sciences
National University of Sciences and Technology
H-12, Islamabad, Pakistan

2021

FORM TH-4

National University of Sciences & Technology

MS THESIS WORK

We hereby recommend that the dissertation prepared under our supervision by: Mr. Naeem ur Rehman, Regn No. 00000278257 Titled: Pulsatile Flow of Nanofluids Between Concentric Cylinders be accepted in partial fulfillment of the requirements for the award of **MS** degree.

Examination Committee Members

1. Name: DR. MERAJ MUSTAFA HASHMI Signature: _____

2. Name: DR. SYED TAYYAB HUSSAIN SHAH Signature: _____

External Examiner: DR. RIZWAN UL HAQ Signature: _____

Supervisor's Name DR. ASIM AZIZ Signature: _____

_____ 25/02/2021

Head of Department Date

COUNTERSINGED

Date: 25-02-2021

Dean/Principal

Dedicated to
My beloved parents Mushtaq Ur Rehman and Sugran Parveen.

Acknowledgements

In the first place I am thankful to Allah for showering with countless blessings and continuous assistance in every phase of life. I would also like to express my sincere gratitude and superfine warm thanks to my supervisor **Dr. Asim Aziz** for great help and support throughout my MS research, and also for his patience, motivation, enthusiasm, and immense knowledge. His guidance helped me in research and in writing of this thesis. It is not often that one finds an advisor and colleague that always finds the time for listening to the little problems and roadblocks that unavoidably crop up in the course of performing research. I could not have imagined having a better advisor, overseer and mentor for my MS study. His kind support and guidance have been of great value in this study.

I thank **Dr. Syed Tayyab Hussain Shah** for his guidance and valuable advice and friendly help in many respect. His extensive discussions around my work and interesting explorations on difficult concepts have been very helpful for this study. His help and suggestions have made a difference.

I would like to thank my family especially my father **Mushtaq Ur Rehman**, my mother **Sugran Parveen** and my friend **Ahtsham Ul Haq** for being so supportive and for their love.

Abstract

It is perceived that the addition of nanoparticles has increased the heat transfer capabilities of ordinary fluids significantly for both turbulent and laminar flow regimes. This dissertation analyzes the effects of two different types carbon nanotubes (CNTs) on flow and heat transfer characteristics of viscous fluid between two concentric cylinders in the presence of thermal radiation effects. The flow of MHD viscous fluid in a Darcy type porous medium is driven by the pressure gradient, assumed as a periodic function of time. The fluid is taken as optically thick and radiations can travel only a short distance within the fluid. The magnetic field is applied perpendicular to the direction of flow and the induced magnetic field is considered negligible. The conventional governing equations are based upon partial differential equations affected by the viscosity of the base fluid, effective thermal conductivity, and thermophysical characteristics of CNTs nanoparticles. The exact solutions are obtained in the form of the modified Bessel functions of the first and second kind. The effect of the flow control parameters like thermal radiation parameter N_r, nanoparticles volume fraction ϕ, and Darcy number D_a are illustrated through graphs. Based on a comprehensive analysis, it is concluded that the addition of single-walled carbon nanotubes (SWCNTs) provides higher velocity and temperature distribution of nanofluid when compared with the multi-walled carbon nanotubes (MWCNTs).

Contents

Chapter 1

Introduction

The most significant and basic natural and industrial processes are the flow through a cylindrical shape. For example, water distribution through pipes, heart siphoning, blood distribution through cylindrical-shaped blood vessels, gas distribution through iron pipes and ducts, automated food processing, heat exchangers, cooling systems, refrigeration, chemical plants, solar collectors, nuclear reactor system, optical modulators, optical switches. The use of cylindrical forms for all such processes is to decrease the drag force with the surface so the fluid can move easily. Though in certain cases flow through cylinders stabilizes by application of external forces. There are many ways to control or generate fluid movement in cylindrical form, pressure is an effective process to improve the tendency of fluid movement. This phenomenon of flow under pressure is known as pulsatile flow. Keeping the aforementioned in view there have been several experiments performed to understand the characteristics of the pulsatile flow. Richardson and Tyler [1] through their model confirmed the presence of maximum flow velocity close to the pipe rim. Later analyses of Womersley [2] and Uchida [3] verified this result in the study of sinusoidal motion in the horizontal pipe containing incompressible oscillating fluid. The fundamental concepts and analytical results for the velocity profile for unsteady flow in cylindrical pipes are presented by Atabek and Chang [4]. Kakac [5] obtained solutions within the case of forced flow between two adjacent surfaces. Stud et al. [6] observed the influence of a dynamic magnetic field in blood flow and found that the application of an effective magnetic field improves the

blood flow rate. Sucec [7] used the finite difference method to analyze the response functions of the wall temperature and the mean temperature due to the laminar fluid flow. Agrawal and Anwarudin [8] presented a mathematical model that discusses how magnetic force affects blood flow through channels with identical branches. They have found that the magnetic force can be used as a blood pump to wear heart processes to treat artery diseases. Similarly, Chaturani and Palanisamy [9] describe the effect of oscillatory body acceleration on blood movement. They have evaluated the analytical result of the pulsatile motion of blood flow through finite Laplace and Hankel transform methods. It is noteworthy that an increase in the velocity provides the transformation of fluid momentum from the tube axis to the closest tube wall area. Majdalani and Chibli [10] obtained the results of the momentum equations governing the pulsative flow through a cylindrical duct where pressure was replaced by the sum of pulses described in terms of the Fourier series. Shahed [11] achieved the closed-form solutions using Laplace and Hankel transforms for flow inside the porous channel with the pulsatile motion of blood flow. He stated that the velocity distribution is an increasing function of the permeability parameter and shows a comparative analysis for the limiting case. Yakhot and Grinberg [12] examined the impact of an increase in the velocity and the pressure gradient with a phase difference. Eldesoky and Mousa [13] discussed the peristaltic flow of non-Newtonian Maxwell fluid via permeable media in a cylinder. Hassan and Mohammed [14] analyzed the pulsatile flow of a non-Newtonian fluid within a non-Darcy porous medium between two permeable parallel sheets. In the case of pulsatile flow, Majdalani [15] achieved the exact solutions for optimizing the velocity distribution and the stress coefficient.

Heat transfer caused by fluid flow is a thrust area of research in the field of fluid mechanics. Therefore processes including heat transfer have been given great attention by the researchers in recent years. Analysis of any model which includes heat transfer is influenced by many factors like the geometry of the flow, a viscosity of the fluid, flow medium, boundary conditions, thermal conductivity, etc. Nanofluids are reported to enhance the poor thermal conductivity of ordinary fluids and improve

their thermal performance. This invention was first conceived by Choi et al. [16] and showed an anomalous enhancement in thermal conductivity due to the suspensions of nanoparticles. They noticed that nanomaterial gives the highest enhancement of thermal conductivity and coefficient of conventional heat transfer of ordinary fluid. Nanofluids require some physical physiognomies of fluid and nanoparticles such as heat diffusivity, viscosity, heat conductivity and comparable coefficients of convective heat transfer [17–19]. Buongiorno [20] introduced the carriage of nanofluid through an essential slip mechanism. Researchers discussed the nanofluid flow phenomena for different types of fluids and nanoparticles for different geometries [21–26].

Carbon nanotubes (CNTs) are thin, long cylinders of carbon atoms with a diameter usually measured by nanometers (0.7-50 nm). There are two kinds of carbon nanotubes based upon the number of graphene layers. These are called single-walled (SWCNTs) and multiple-walled (MWCNTs) carbon nanotubes respectively. In several fields of technology, such as electronics, optics, electronic sensors, composite materials, biosensors, and in materials science applications, carbon nanotubes are used to improve thermal performance. Analysis of the characteristics of CNTs on the fluid movement and heat transportation of nanofluid is therefore very significant. The properties of SWCNTs and MWCNTs are similar but have some noticeable variations as well. The terminology of CNTs was first introduced by Iijima [27] by producing the MWCNTs. The reliable use of CNTs for electrical technologies were proposed by Ramasubramanian et al. [28]. Xue [29] discussed the theoretical and experimental theories of CNT's. Ding et al. [30] studied the heat transfer behavior of CNTs nanofluids flowing through a horizontal pipe. They found an important enhancement in the convective heat transfer and observed that the enhancement depends on the Reynolds number and solid volume fraction of CNTs. Kamali and Binesh [31] explored improvement in heat transport by using the non-Newtonian model for Nanofluids with CNTs in a straight pipe. The results showed the heat transfer coefficient is highest near the boundary region due to the non-Newtonian behavior of CNTs based nanofluid. Wang et al. [32] set up an experimental investigation to study the heat transfer of nanofluids-based upon

CNTs. They showed that the nanofluids at low concentration enhance the heat transfer at the boundary. Hayat et al. [33] studied rotating fluid flow through CNTs, using the permeable medium of Darcy Frochheimer. Manevitch et al. [34] investigate the effect of nonlinear radiation and optical motions on SWCNT. Mahanthesh et al. [35] investigated the effect of nonlinear thermal radiation with Marangoni convection in carbon nanotubes(CNTs) based on nanofluids flow. Nadeem [36] investigated the peristaltic flow in an inclined cylindrical form pipe having porous walls in the presence of SWCNT. He observed that bolus increases by adding carbon nanotubes. Haq et al. [37] presented an MHD slip flow with convective heat transport in the presence of single and multi-walled carbon nanotubes. They found that the presence of CNTs plays an significant role in the improvement of thermal conductivity. Hamid et al. [38] studied the flow behavior of CNTs nanofluid in a partially heated rectangular fin-shaped cavity with an inner cylindrical barrier. They showed that carbon nanotubes have unique physical and chemical characteristics. Thus, CNTs nanoparticles can be considered as the best enhancing heat transfer candidate. Xiao et al. [39] investigated the natural free-convection flow in a perpendicular cylinder of viscous carbon nanotubes nanofluids in the presence of a magnetic field by observing memory effects for the thermal equation using Fourier's law. Oktay et al. [40] examined the mixed convection and entropy generation using local thermal nonequilibrium (LTNE) model in an annulus with a rotating heated inner cylinder for SWCNT–water nanofluid flow. They showed that the inclusion of SWCNTs to based fluid leads to a decrease in the value of minimum total entropy generation. Recent investigations studying carbon nanotubes nanofluid flow may be found in [41–43].

The principal objective of present research is to analyze the pulsatile flow and heat transfer of thermally radiative CNTs based nanofluid. The nanofluid is flowing through two concentric cylinders in a Darcy type porous medium. Flow is formed by means of the oscillating pressure gradient. The standard governing equations are developed based on basic momentum equation and heat equation and then solved analytically to receive the exact solutions in the form of the Bessel's functions. The obtained

results for temperature distribution, velocity distribution and dimensionless pressure are described graphically through variant in physical parameters. Dominant differences can be observed in temperature and velocity profiles for both water-based SWCNTs and water-based MWCNTs nanofluids. In addition, the dimensionless pressure gradient is calculated for different time values.

The thesis is arranged as follows:

Chapter 2 presents basic definitions of fluid flow, heat transfer and basic governing equations of continuity, momentum and energy in cylindrical coordinates. These preliminary concepts are then employed in the subsequent chapters. **Chapter 3** presents the mathematical model for flow of Magnetohydrodynamics pulsatile flow of CNT based nanofluids between two concentric cylinders. The analysis is carried on engine oil based carbon nanotubes. The associated governing system of partial differential equations are then transformed into ordinary differential equations and solved analytically in term of Bessel functions. The behaviour of physical parameters which influence the model is delineated in the graphs. In **Chapter 4**, the mathematical model presented in **Chapter 3** is extended by including the effect of thermal radiation and porous medium. The obtained results are presented in the form of graphs. **Chapter 6** concludes the research work and discusses possible future work.

Chapter 2

Preliminaries and Basic Equations

This chapter contains specific concepts of fluid flow, flow forms and specific equations with respect to fluid flow and heat transfer. It also provides an introduction to nanofluids and some of the physical parameters of nanofluid.

2.1 Fluid and Fluid Flow

A fluid is a particular kind of matter that has the ability to continuously deform itself when shear stress is applied on it. This includes liquids, gases, plasma's and some plastic solids. The phenomenon in which fluid continuously deforms itself is known as fluid flow.

2.2 Steady and Unsteady Flow

A flow in which properties of fluid at a particular point remain constant with time is known as steady flow. Mathematically, it is stated as

$$\frac{D\gamma}{Dt} = 0, \tag{2.1}$$

where t is time and γ is any fluid property. A flow in which fluid at a particular point changes its properties with time is known as unsteady flow. Mathematically, it is stated as

$$\frac{D\gamma}{Dt} \neq 0. \tag{2.2}$$

2.3 Laminar and Turbulent Flow

Laminar flow is a kind of fluid flow in which fluid moves smoothly in parallel layers. The path lines of fluid particles do not cross each other. This flow usually occurs while dealing with low Reynolds number. The fluid flow in which fluid particles continuously changes their direction is known as turbulent flow.

2.4 Compressible and In-compressible Flow

A fluid flow in which the density of the fluid remains constant is known as the incompressible flow, i.e.,

$$\frac{D\rho}{Dt} = 0, \tag{2.3}$$

where, ρ indicates the fluid density and $\frac{D}{Dt}$ denotes the material derivative which is defined as

$$\frac{D}{Dt} = \frac{\partial}{\partial t} + \mathbf{V}.\nabla. \tag{2.4}$$

A fluid flow in which the fluid density varies with time is known as compressible flow.

2.5 Axi-symmetric Flow

An axi-symmetric flow is the one in which all the streamlines are positioned symmetrically around the axis. In this flow both pressure term p and the cylindrical velocity components v_r, v_θ, v_z are independent of the angular variable θ.

2.6 Pulsatile Flow

In fluid dynamics, a flow with periodic variation is known as pulsatile flow. The cardiovascular system of chordate animals is a very good example where pulsatile flow is found.

2.7 Viscosity

Viscosity is a quantity that shows fluid opposition to the deformation or shear stresses and is measured by the coefficient of viscosity, μ. Mathematically, it is written as

$$\mu = \frac{shear\ stress}{deformation\ rate}. \tag{2.5}$$

In the above equation μ is absolute or dynamic viscosity. The other type of viscosity is called as Kinematic viscosity, ν, which is a ratio of dynamic viscosity to density of the fluid and has a following expression

$$\nu = \frac{\mu}{\rho}. \tag{2.6}$$

The fluids having non-zero viscosity are known as Viscous fluids while those having zero dynamic viscosity are known as inviscid fluids.

2.8 Newton's Law of Viscosity

This law creates a relationship between stress on fluid and the rate of shear strain. In other words, shear stress is proportional (linearly) to velocity gradient. Mathematically it can be written as

$$\tau_{\mathrm{xy}} = \mu \frac{du}{dy}. \tag{2.7}$$

Here, $\frac{du}{dy}$ is shear strain rate, τ indicates the shear stress and μ is the coefficient of viscosity.

2.9 Newtonian and Non-Newtonian Fluids

Newtonian fluids are those fluids which obey the Newton's law of viscosity. Most ordinary Newtonian fluids are air, water, organic solvents, gasoline etc. The fluids having the property that, the shear stress is not linearly proportional to the rate of deformation are called as non-Newtonian fluids. Some of the substances that show non-Newtonian behavior are ketchup, jams, yogurt, butter, gums, soup solution, cement slurry, blood, saliva etc.

2.10 Continuity Equation

Continuity equation is based on law of conservation of mass which states that mass can neither be generated nor demolished but can be converted from one profile to another inside a control volume. Mathematically, it is written as

$$\frac{\partial \rho}{\partial t} + \nabla.(\rho \mathbf{V}) = 0, \tag{2.8}$$

where V represents velocity vector and ∇ is the differential operator. If ρ is constant, then (2.8) becomes

$$\nabla.\mathbf{V} = 0, \tag{2.9}$$

Continuity equation in cylindrical coordinates with velocity field $\vec{V}$=(v_r, v_θ, v_z) is

$$\frac{\partial \rho}{\partial t} + \frac{1}{r}\frac{\partial}{\partial r}(\rho r v_r) + \frac{1}{r}\frac{\partial}{\partial \theta}(\rho v_\theta) + \frac{\partial}{\partial z}(\rho v_z) = 0. \tag{2.10}$$

2.11 Momentum Equation

Law of conservation of momentum states that net force acting on a particle in fluid is equal to time rate of change of linear momentum. Momentum equation is derived by generalizing the law of conservation of momentum. Mathematical form of this law is known as Navier-Strokes equation and has the form

$$\rho \frac{D\mathbf{V}}{Dt} = \nabla.\tau + \rho \mathbf{g}, \tag{2.11}$$

where, τ is Cauchy stress tensor, $\rho\mathbf{g}$ is body force per unit mass and $\nabla.\tau = (-\nabla P + \mu\nabla^2\mathbf{V})$ represent surface forces. Then (2.11) becomes

$$\rho \frac{D\mathbf{V}}{Dt} = -\nabla P + \mu\nabla^2\mathbf{V} + \rho\mathbf{g}. \tag{2.12}$$

The general form of Navier-Strokes equation, with velocity vector expanded as $\vec{V}$ = (u, v, w), one can write the vector equation (2.12) in cylindrical coordinates as

$r-component$:

$$\rho\left[\frac{\partial v_r}{\partial t}+v_r\frac{\partial v_r}{\partial r}+\frac{v_\theta}{r}\frac{\partial v_r}{\partial \theta}-\frac{{v_\theta}^2}{r}+v_z\frac{\partial v_r}{\partial z}\right]$$
$$=-\frac{\partial p}{\partial r}+\mu\left[\frac{1}{r}\frac{\partial}{\partial r}\left(r\frac{\partial v_r}{\partial r}\right)-\frac{v_r^2}{r^2}-\frac{2}{r^2}\frac{\partial v_r}{\partial \theta}+\frac{1}{r^2}\frac{\partial^2 v_r}{\partial \theta^2}+\frac{\partial^2 v_r}{\partial z^2}\right]$$
$$+\frac{\mu}{3}\frac{\partial}{\partial r}\left[\frac{1}{r}\frac{\partial(rv_r)}{\partial r}+\frac{1}{r}\frac{\partial v_\theta}{\partial \theta}+\frac{\partial v_z}{\partial z}\right]+\rho g_r, \tag{2.13}$$

$\theta-component$:

$$\rho\left[\frac{\partial v_\theta}{\partial t}+v_r\frac{\partial v_\theta}{\partial r}+\frac{v_\theta}{r}\frac{\partial v_\theta}{\partial \theta}+\frac{v_r v_\theta}{r}+v_z\frac{\partial v_\theta}{\partial z}\right]$$
$$=-\frac{1}{r}\frac{\partial p}{\partial \theta}+\mu\left[\frac{1}{r}\frac{\partial}{\partial r}\left(r\frac{\partial v_\theta}{\partial r}\right)+\frac{1}{r^2}\frac{\partial^2 v_\theta}{\partial \theta^2}-\frac{v_\theta^2}{r^2}+\frac{2}{r^2}\frac{\partial v_\theta}{\partial \theta}+\frac{\partial^2 v_\theta}{\partial z^2}\right]$$
$$+\frac{\mu}{3}\frac{\partial}{\partial \theta}\left[\frac{1}{r}\frac{\partial(rv_r)}{\partial r}+\frac{1}{r}\frac{\partial v_\theta}{\partial \theta}+\frac{\partial v_z}{\partial z}\right]+\rho g_\theta, \tag{2.14}$$

$z-component$:

$$\rho\left[\frac{\partial v_z}{\partial t}+v_r\frac{\partial v_z}{\partial r}+\frac{v_\theta}{r}\frac{\partial v_z}{\partial \theta}+v_z\frac{\partial v_z}{\partial z}\right]$$
$$=-\frac{\partial p}{\partial z}+\mu\left[\frac{1}{r}\frac{\partial}{\partial r}\left(r\frac{\partial v_z}{\partial r}\right)+\frac{1}{r^2}\frac{\partial^2 v_z}{\partial \theta^2}+\frac{\partial^2 v_z}{\partial z^2}\right]$$
$$+\frac{\mu}{3}\frac{\partial}{\partial z}\left[\frac{1}{r}\frac{\partial(rv_r)}{\partial r}+\frac{1}{r}\frac{\partial v_\theta}{\partial \theta}+\frac{\partial v_z}{\partial z}\right]+\rho g_z. \tag{2.15}$$

2.12 Heat Transfer

Heat transfer is a process in which transferring of thermal energy occurs due to temperature difference between the physical systems. There are three different ways of heat transfer, conduction, convection, radiation.

2.12.1 Conduction

The process of heat transfer which occurs because of the molecular collisions is known as conduction. Fourier developed a law known as Fourier's law of heat conduction. Mathematical form of the law is

$$Q=-\kappa A\frac{dT}{dx}. \tag{2.16}$$

Here Q is heat flow rate, κ is thermal conductivity, $\frac{dT}{dx}$ is temperature gradient, T is temperature and A is cross-sectional area.

2.12.2 Convection

It is defined as heat transfer in fluids from a part with high temperature to a part where temperature is comparatively low. In convection, Newton's law of cooling governs heat transfer rate with the expression

$$Q = hA(T - T_\infty). \tag{2.17}$$

Here, A is cross-sectional area, h is coefficient of convection and T_∞ is temperature of the outside environment.

2.12.3 Radiation

Radiation occurs by photons of light or waves emitted from a surface volume. Radiation can happen in vacuum also. Stefan-Boltzmann law is used to calculate the amount transfer through radiation. Mathematically

$$Q = \sigma.T^4. \tag{2.18}$$

Here σ denotes Stefan-Boltzmann's constant.

2.13 Energy Equation

This equation is formed by generalizing the first law of thermodynamics which ensures that rate of change of fluid's energy inside a control volume is equals to rate of work done due to body or surface forces and rate of heat addition. The governing equation which includes energy conservation can be composed as

$$\rho c_p \frac{D\mathbf{T}}{Dt} = \nabla.(\kappa \nabla T) + f.\mathbf{T}, \tag{2.19}$$

In the above expression, κ is thermal conductivity of the fluid and c_p denote specific heat at a constant temperature and f is body or surface force. In cylinder coordinates system equation 2.19 will become

$$\rho c_p \left[\frac{\partial T}{\partial t} + v_r \frac{\partial T}{\partial r} + \frac{v_\theta}{r}\frac{\partial T}{\partial \theta} + v_z \frac{\partial T}{\partial z}\right] = \kappa \left[\frac{1}{r}\frac{\partial T}{\partial r} + \frac{\partial^2 T}{\partial r^2} + \frac{1}{r^2}\frac{\partial^2 T}{\partial \theta^2} + \frac{\partial^2 T}{\partial z^2}\right]. \quad (2.20)$$

2.14 Magnetohydrodynamics (MHD)

Branch of engineering in which behavior of magnetic field in electrically conducting fields is studied is known as Magnetohydrodynamics. Combination of equations of motion and Maxwell's equation of electromagnetism results in the set of equations which represents MHD flow. The momentum equation (2.11) with electromagnetic force term for MHD fluid flow is

$$\rho \frac{D\mathbf{V}}{Dt} = \nabla.\tau + (\mathbf{J} \times \mathbf{B}), \quad (2.21)$$

where $\mathbf{J}$ shows density of current and $\mathbf{B}$ is total magnetic field which has following expression

$$\mathbf{B} = \mathbf{B} + \mathbf{B}_1, \quad (2.22)$$

where $\mathbf{B}_1$ is the induced magnetic field. Here $\mathbf{B}_1$ is considered very small in comparison with external magnetic field and thus it can be ignored. This is justified for MHD flow with small Reynolds number. By Ohms law, $\mathbf{J}$ is given as

$$\mathbf{J} = \sigma(\mathbf{E} + \mathbf{V} \times \mathbf{B}), \quad (2.23)$$

where σ is electrical conductivity and $\mathbf{E}$ is electrical field. After simplification equation (2.23) becomes

$$\mathbf{J} \times \mathbf{B} = \left[0, 0, -\sigma {B_o}^2 v_z\right]. \quad (2.24)$$

Using equation (2.23), momentum equation (2.21) becomes

$$\rho \frac{D\mathbf{V}}{Dt} = \nabla.\tau - \sigma {B_o}^2 v_z. \quad (2.25)$$

2.15 Porous Medium

A porous medium (or porous material) is a material composed of a persistent solid part, called solid matrix, and the remaining pore space (or void space) that can be filled with one or more fluids (e.g. oil, water and gas). Typical examples of a porous medium are soil, karstic limestone, sand, foam cemented sandstone, bread, rubber, lungs or kidneys.

2.16 Nanofluids

Nanofluids are a special kind of fluids that have improved thermal conductivity.Nanofluids include base fluid (water, oil, ethynol, etc.) in which particles of a nano-meter-sized scale (1-100 nm) are suspended. Metals (Cu, Al, Ag), oxides (Al2O3, CuO), carbides (SiC, TiC) and carbon nano-tubes form several common nanoparticles used to create nanofluids.

2.17 Physical Parameters of Nanofluid

Below are some of the physical parameters used in nanofluid discussion

2.17.1 Viscosity

Viscosity of nanofluid is given by Brinkman [44] as

$$\mu_{nf} = \frac{\mu_f}{(1-\phi)^{2.5}}. \tag{2.26}$$

Here, ϕ is nanoparticle volume fraction coefficient and μ_f is dynamic viscosity of base fluid.

2.17.2 Density

Density of nanofluid is given by Khanafer et al. [45] as

$$\rho_{nf} = (1-\phi)\,\rho_f + \phi\rho_s. \tag{2.27}$$

Here, ρ_f is the base fluid density and ρ_s is the density of solid particles.

2.17.3 Specific heat

Specific heat of nanofluid is given by Khanafer et al. [45] as

$$(\rho c_p)_{nf} = (1-\phi)\,(\rho c_p)_f + \phi(\rho c_p)_s. \tag{2.28}$$

In the above equation, $(c_p)_s$ is solid nanoparticle specific heat and $(c_p)_f$ is basefluid specific heat capacity.

2.17.4 Thermal Conductivity

It is given by Xue [29] as

$$\kappa_{nf} = \kappa_f \left[\frac{1-\phi+2\phi\left(\frac{\kappa_s}{\kappa_s-\kappa_f}\right)\ln\left(\frac{\kappa_s+\kappa_f}{2\kappa_f}\right)}{1-\phi+2\phi\left(\frac{\kappa_f}{\kappa_s-\kappa_f}\right)\ln\left(\frac{\kappa_s+\kappa_f}{2\kappa_f}\right)} \right]. \tag{2.29}$$

In the above equation, the thermal conductivity κ_{nf} of nanofluid is a function solid volume fraction ϕ, thermal conductivity of the base fluid κ_f and thermal conductivity of the nanoparticle κ_s.

2.18 Carbon Nanotube (CNT)

Carbon nanotubes (CNTs) are thin, long cylinders of carbon atoms with a diameter usually measured by nanometers (0.7-50 nm). There are two kinds of carbon nanotubes based upon the number of graphene layers. These are called single-walled (SWCNTs) and multiple-walled (MWCNTs) carbon nanotubes respectively.

2.18.1 Single-walled Carbon Nanotube (SWCNT)

A single-walled carbon nanotube (SWCNT) is a seamless cylinder which consists of only one layer of graphene. It shows impressively unique electrical properties.

2.18.2 Multi-walled Carbon Nanotube (MWCNT)

A multi-walled carbon nanotube (MWCNT) is also cylindrical in shape, with multiple concentric layers of graphene composing it. These are comparatively complex structure and variety.

Chapter 3

MHD Pulsatile Flow of Engine Oil Based Carbon Nanotubes Between Two Concentric Cylinders

This chapter covers a review of the work of Haq et al. [37]. It describes the unidirectional MHD flow of viscous fluid with heat transport in the presence of carbon nanotubes(SWCNTs and MWCNTs). Constitutive equations of conservation of mass, momentum equation and energy are based upon PDEs that contain thermos-physical characteristics of both nanoparticles. Section 3.1 deals with the mathematical formulation of the flow and heat transfer model. Sections 3.2 and 3.3 are about the problem solution and the pressure calculation respectively. Section 3.4 deals with graphical results along with their discussions.

3.1 Mathematical Formulation

An incompressible, viscous fluid is flowing between two concentric ducts as shown in Figure 3.1. The pulsatile pressure gradient is applied in the z-direction to move the fluid within the given channel. The magnetic field B_o is taken along r-direction. The constitutive equations for conservation of mass, momentum and energy equations for the fluid are given in equations (2.9), (2.12) and (2.19), respectively. After neglecting all the body forces and including the Magnetohydrodynamics effect, the momentum equation (2.12) and energy equation (2.19) for the nanofluid reduced to the form

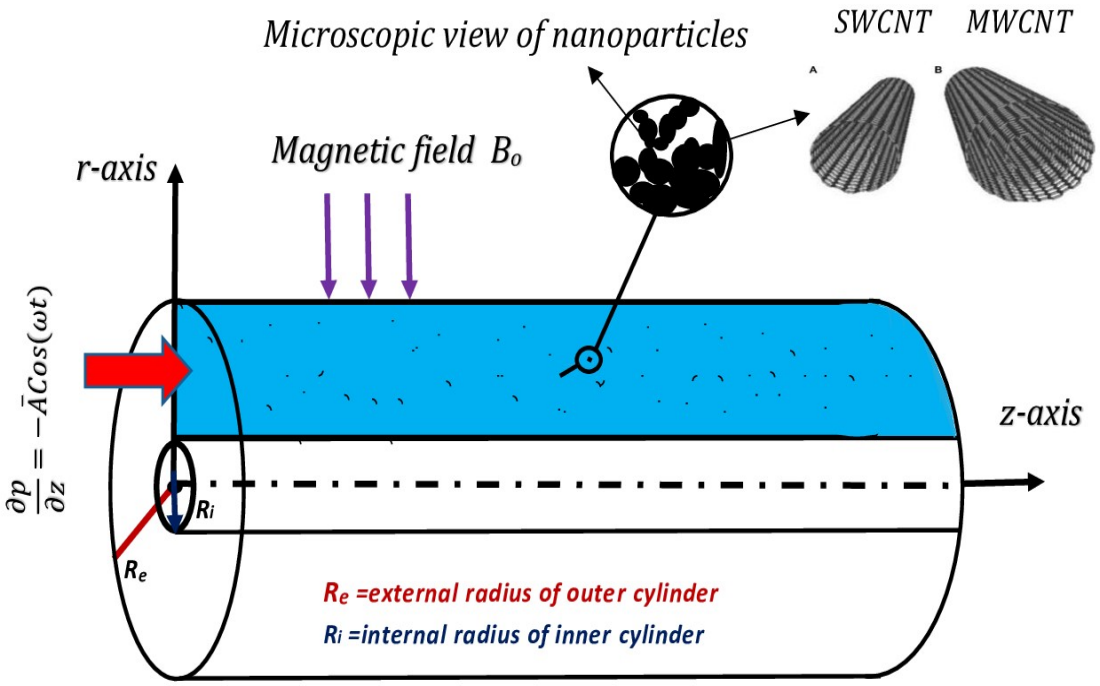

Figure 3.1: Flow field geometry.

$$\rho_{nf}\left[\frac{\partial \vec{V}}{\partial t} + \vec{V}.\nabla\vec{V}\right] = -\nabla P + \mu_{nf}\nabla^2\vec{V} + \left(\vec{J}\times\vec{B}\right), \tag{3.1}$$

$$(\rho c_p)_{nf}\left[\frac{\partial T}{\partial t} + \vec{V}.\nabla T\right] = \kappa_{nf}\nabla^2 T. \tag{3.2}$$

In cylindrical coordinates system, equations (3.1) and (3.2) will become

$$\rho_{nf}\left[\frac{\partial v_r}{\partial t}+v_r\frac{\partial v_r}{\partial r}+v_z\frac{\partial v_r}{\partial z}\right] = -\frac{\partial p}{\partial r}+\mu_{nf}\left[\frac{1}{r}\frac{\partial v_r}{\partial r}+\frac{\partial^2 v_r}{\partial r^2}+\frac{\partial^2 v_r}{\partial z^2}-\frac{v_r}{r^2}\right], \tag{3.3}$$

$$\rho_{nf}\left[\frac{\partial v_z}{\partial t}+v_r\frac{\partial v_z}{\partial r}+v_z\frac{\partial v_z}{\partial z}\right] = -\frac{\partial p}{\partial z}+\mu_{nf}\left[\frac{1}{r}\frac{\partial v_z}{\partial r}+\frac{\partial^2 v_z}{\partial r^2}+\frac{\partial^2 v_z}{\partial z^2}\right]-\sigma_f {B_o}^2 v_z, \tag{3.4}$$

$$(\rho c_p)_{nf}\left[\frac{\partial T}{\partial t}+v_r\frac{\partial T}{\partial r}+v_z\frac{\partial T}{\partial z}\right] = \kappa_{nf}\left[\frac{1}{r}\frac{\partial T}{\partial r}+\frac{\partial^2 T}{\partial r^2}+\frac{\partial^2 T}{\partial z^2}\right]. \tag{3.5}$$

In above equations $(\rho c_p)_{nf}$ is the specific heat capacity of nanofluid, ρ_{nf} is density of nanofluid, μ_{nf} is the viscosity of nanofluid, κ_{nf} is the thermal conductivity of nanofluid and σ_{nf} is the electric conductivity of the nanofluid. Where T_f is the fluid temperature and p represent the pressure. The theoretical framework for CNTs nanofluid was introduced by Xue [29] and is given as

$$\rho_{nf} = (1-\phi)\,\rho_f + \phi\rho_{CNT}, \tag{3.6}$$

$$(\rho c_p)_{nf} = (1-\phi)\,(\rho c_p)_f + \phi(\rho c_p)_{CNT}, \tag{3.7}$$

$$\frac{\kappa_{nf}}{\kappa_f} = \frac{1-\phi+2\phi\left(\frac{\kappa_{CNT}}{\kappa_{CNT}-\kappa_f}\right)\ln\left(\frac{\kappa_{CNT}+\kappa_f}{2\kappa_f}\right)}{1-\phi+2\phi\left(\frac{\kappa_f}{\kappa_{CNT}-\kappa_f}\right)\ln\left(\frac{\kappa_{CNT}+\kappa_f}{2\kappa_f}\right)}, \tag{3.8}$$

$$\mu_{nf} = \frac{\mu_f}{(1-\phi)^{2.5}}. \tag{3.9}$$

In above expressions ρ_f represent the density of fluid, κ_f represent the thermal conductivity of fluid and μ_f represent the dynamic viscosity of the working fluid. Where κ_{CNT} and c_{CNT} represent the thermal conductivity and heat capacity of the carbon nanotubes. ϕ is the nanoparticles concentration. In view of aforementioned quantities,

equations (3.3)-(3.5) are reduced to

$$\left((1-\phi)\,\rho_f+\phi\rho_{CNT}\right)\left[\frac{\partial v_r}{\partial t}+v_r\frac{\partial v_r}{\partial r}+v_z\frac{\partial v_r}{\partial z}\right]$$
$$=-\frac{\partial p}{\partial r}+\frac{\mu_f}{(1-\phi)^{2.5}}\left[\frac{1}{r}\frac{\partial v_r}{\partial r}+\frac{\partial^2 v_r}{\partial r^2}+\frac{\partial^2 v_r}{\partial z^2}-\frac{v_r}{r^2}\right], \tag{3.10}$$

$$\left((1-\phi)\,\rho_f+\phi\rho_{CNT}\right)\left[\frac{\partial v_z}{\partial t}+v_r\frac{\partial v_z}{\partial r}+v_z\frac{\partial v_z}{\partial z}\right]$$
$$=-\frac{\partial p}{\partial z}+\frac{\mu_f}{(1-\phi)^{2.5}}\left[\frac{1}{r}\frac{\partial v_z}{\partial r}+\frac{\partial^2 v_z}{\partial r^2}+\frac{\partial^2 v_z}{\partial z^2}\right]-\sigma_f {B_o}^2 v_z, \tag{3.11}$$

$$\left((1-\phi)\,(\rho c_p)_f+\phi(\rho c_p)_{CNT}\right)\left[\frac{\partial T}{\partial t}+v_r\frac{\partial T}{\partial r}+v_z\frac{\partial T}{\partial z}\right]$$
$$=\kappa_{nf}\left[\frac{1}{r}\frac{\partial T}{\partial r}+\frac{\partial^2 T}{\partial r^2}+\frac{\partial^2 T}{\partial z^2}\right]. \tag{3.12}$$

The associated initial and boundary conditions of the model are:
At $t=0$

$$v_r(r,z,0)=v_z(r,z,0)=0, \quad \text{and} \quad p(r,z,0)=T_f(r,z,0)=0. \tag{3.13}$$

At outer cylinder

$$v_r(1,z,t)=v_z(1,z,t)=0, \quad \text{and} \quad \frac{\partial T_f}{\partial r}(1,z,t)=0. \tag{3.14}$$

At inner cylinder

$$v_r(\frac{R_i}{R_e},z,t)=v_z(\frac{R_i}{R_e},z,t)=0, \quad \text{and} \quad T_f(\frac{R_i}{R_e},z,t)=1. \tag{3.15}$$

To non-dimensionlize the equations (3.10)-(3.12) subject to initial boundary conditions (3.13)-(3.15) following set of dimensionless variables are introduced as

$$v_r=\frac{v_r'}{\omega R_e}, \quad v_z=\frac{v_z'}{\omega R_e}, \quad r=\frac{r'}{R_e}, \quad z=\frac{z'}{R_e},$$
$$t=\omega t', \quad p=\frac{p'}{R_e^2\omega^2\rho_f}, \quad T=\frac{T'-T_f}{T_i-T_f}. \tag{3.16}$$

By using the variables defined in equation (3.16) to transform the equations (3.10)-(3.12) into non-dimensional form and here we ignore prime for simplicity.

$$\left[(1-\phi)+\left(\frac{\rho_{CNT}}{\rho_f}\right)\phi\right]\left[\frac{\partial v_r}{\partial t}+v_r\frac{\partial v_r}{\partial r}+v_z\frac{\partial v_r}{\partial z}\right] = -\frac{\partial p}{\partial r}+\frac{\mu_f}{(1-\phi)^{2.5}\,\omega {R_e}^2\rho_f}\left[\frac{1}{r}\frac{\partial v_r}{\partial r}+\frac{\partial^2 v_r}{\partial r^2}+\frac{\partial^2 v_r}{\partial z^2}-\frac{v_r}{r^2}\right], \tag{3.17}$$

$$\left[(1-\phi)+\left(\frac{\rho_{CNT}}{\rho_f}\right)\phi\right]\left[\frac{\partial v_z}{\partial t}+v_r\frac{\partial v_z}{\partial r}+v_z\frac{\partial v_z}{\partial z}\right] = -\frac{\partial p}{\partial z}+\frac{\mu_f}{(1-\phi)^{2.5}\,\omega {R_e}^2\rho_f}\left[\frac{1}{r}\frac{\partial v_z}{\partial r}+\frac{\partial^2 v_z}{\partial r^2}+\frac{\partial^2 v_z}{\partial z^2}\right]-\frac{\sigma_f B_o^2}{\omega\rho_f}v_z, \tag{3.18}$$

$$\left[(1-\phi)+\left(\frac{(\rho c_p)_{CNT}}{(\,\rho c_p)_f}\right)\phi\right]\left[\frac{\partial T}{\partial t}+v_r\frac{\partial T}{\partial r}+v_z\frac{\partial T}{\partial z}\right] = \frac{\kappa_{nf}}{\omega {R_e}^2\,(\rho c_p)_f}\left[\frac{1}{r}\frac{\partial T}{\partial r}+\frac{\partial^2 T}{\partial r^2}+\frac{\partial^2 T}{\partial z^2}\right]. \tag{3.19}$$

After simplification equations (3.17)-(3.19) reduced to the form

$$A_1\left[\frac{\partial v_r}{\partial t}+v_r\frac{\partial v_r}{\partial r}+v_z\frac{\partial v_r}{\partial z}\right] = -\frac{\partial p}{\partial r}+\frac{1}{(1-\phi)^{2.5}Re_\omega}\left[\frac{1}{r}\frac{\partial v_r}{\partial r}+\frac{\partial^2 v_r}{\partial r^2}+\frac{\partial^2 v_r}{\partial z^2}-\frac{v_r}{r^2}\right], \tag{3.20}$$

$$A_1\left[\frac{\partial v_z}{\partial t}+v_r\frac{\partial v_z}{\partial r}+v_z\frac{\partial v_z}{\partial z}\right] = -\frac{\partial p}{\partial z}+\frac{1}{(1-\phi)^{2.5}Re_\omega}\left[\frac{1}{r}\frac{\partial v_z}{\partial r}+\frac{\partial^2 v_z}{\partial r^2}+\frac{\partial^2 v_z}{\partial z^2}\right]-\frac{M^2}{Re_\omega}v_z, \tag{3.21}$$

$$A_2\left[\frac{\partial T}{\partial t}+v_r\frac{\partial T}{\partial r}+v_z\frac{\partial T}{\partial z}\right] = \frac{A_3}{Pr.Re_\omega}\left[\frac{1}{r}\frac{\partial T}{\partial r}+\frac{\partial^2 T}{\partial r^2}+\frac{\partial^2 T}{\partial z^2}\right]. \tag{3.22}$$

The dimensionless parameters appearing in Eqs. (3.20)-(3.22) are defined as

$$Pr=\frac{\mu_f(c_p)_f}{\kappa_f}, \qquad M=R_eB_o\sqrt{\frac{\sigma_f}{\mu_{\mathrm{f}}}}, \qquad Re_\omega=\alpha^2=\frac{\omega R_e^2}{\nu_f}. \tag{3.23}$$

The coefficients A_1, A_2 and A_3 are defined as

$$A_1 = \left[(1-\phi) + \left(\frac{\rho_{CNT}}{\rho_f}\right)\phi\right], \tag{3.24}$$

$$A_2 = \left[(1-\phi) + \left(\frac{(\rho c_p)_{CNT}}{(\rho c_p)_f}\right)\phi\right], \tag{3.25}$$

$$A_3 = \frac{\kappa_{nf}}{\kappa_f} = \frac{1-\phi+2\phi\left(\frac{\kappa_{CNT}}{\kappa_{CNT}-\kappa_f}\right)\ln\left(\frac{\kappa_{CNT}+\kappa_f}{2\kappa_f}\right)}{1-\phi+2\phi\left(\frac{\kappa_f}{\kappa_{CNT}-\kappa_f}\right)\ln\left(\frac{\kappa_{CNT}+\kappa_f}{2\kappa_f}\right)}. \tag{3.26}$$

The dimensionless form of boundary conditions are

$$v_z = 0, \quad \frac{\partial T}{\partial r} = 0, \qquad at \quad r = 1, \tag{3.27}$$

$$v_z = 0, \qquad T = 1, \qquad at \quad r = \frac{R_i}{R_e} = R^*. \tag{3.28}$$

Assume the flow is fully developed and the velocity field is of the form

$$\vec{V} = [0, 0, v_z(r, z, t)]. \tag{3.29}$$

In case of axis-symmetric flow equations (3.20) and (3.22) becomes,

$$A_1\frac{\partial v_z}{\partial t} = -\frac{\partial p}{\partial z} + \frac{A_4}{Re_\omega}\left[\frac{1}{r}\frac{\partial v_z}{\partial r} + \frac{\partial^2 v_z}{\partial r^2}\right] - \frac{M^2}{Re_\omega}v_z, \tag{3.30}$$

$$A_2\left[\frac{\partial T}{\partial t} + v_z\frac{\partial T}{\partial z}\right] = \frac{A_3}{Pr.Re_\omega}\left[\frac{1}{r}\frac{\partial T}{\partial r} + \frac{\partial^2 T}{\partial r^2} + \frac{\partial^2 T}{\partial z^2}\right]. \tag{3.31}$$

3.2 Solution of the Problem

The problem considered in this study deals with the pulsatile flow and heat transfer, therefore periodic pressure gradient can be expressed as

$$\frac{\partial P}{\partial z} = -ACos(\omega t) = Real(-Ae^{i\omega t}). \tag{3.32}$$

The solution of the velocity profile can be defined as

$$v_z(r, t) = Real\left[f(r)e^{it}\right]. \tag{3.33}$$

In view of above equations, equation (3.30) reduce to the form

$$\frac{d^2f(r)}{dr^2} + \frac{1}{r}\frac{df(r)}{dr} - \frac{1}{A_4}\left(M^2 + i\alpha^2 A_1\right) f(r) = -\frac{A\alpha^2}{A_4}. \tag{3.34}$$

The solution of equation (3.34) is

$$f(r) = C_1 I_0(\zeta r) + C_2 K_0(\zeta r) + \frac{A\alpha^2}{\zeta^2 A_4}, \tag{3.35}$$

where I_o and K_o are the zeroth order modified Bessel functions of 1st and 2nd kind and $\zeta = \sqrt{\frac{1}{A_4}\left(M^2 + i\alpha^2 A_1\right)}$. Equation (3.33) gives the velocity profile as

$$v_z(r,t) = Real\left[C_1 I_0(\zeta r) + C_2 K_0(\zeta r) + \frac{A\alpha^2}{\zeta^2 A_4}\right] e^{it} \tag{3.36}$$

Using boundary conditions (3.13)-(3.15) in the above equation one can find

$$C_1 = -\frac{\alpha^2 BesselK[0,\zeta]A - \alpha^2 BesselK[0,\zeta R^*]A}{\zeta^2 A_4\left(BesselI[0,\zeta R^*]BesselK[0,\zeta] - BesselI[0,\zeta]BesselK[0,\zeta R^*]\right)}, \tag{3.37}$$

$$C_2 = -\frac{-\alpha^2 BesselI[0,\zeta]A + \alpha^2 BesselI[0,\zeta R^*]A}{\zeta^2 A_4\left(BesselI[0,\zeta R^*]BesselK[0,\zeta] - BesselI[0,\zeta]BesselK[0,\zeta R^*]\right)}. \tag{3.38}$$

In order to find the analytical solution of the Eq. (3.31), the solution for the temperature profile is assumed as

$$T(r,z,t) = Real\left[-\gamma^{'} z + \gamma^{'} g(r) e^{it} + 1\right], \tag{3.39}$$

where $\gamma^{'} = \frac{Re}{L}$. Equation (3.31) together with equation (3.39) reduces to

$$\frac{d^2g(r)}{dr^2} + \frac{1}{r}\frac{dg(r)}{dr} - i\frac{A_2 Pr\alpha^2}{A_3} g(r) = \frac{A_2 Pr\alpha^2}{A_3} f(r). \tag{3.40}$$

The solution of Eq. (3.40) is

$$\begin{aligned} T(r,z,t) = Real[-\gamma^{'} z + \gamma^{'}[-iC_1 I_0(\zeta r) - iC_2 K_0(\zeta r) + C_3 I_0(\xi r) \\ + C_4 K_0(\xi r) - i\frac{A\alpha^2}{\zeta^2 A_4}]e^{it} + 1], \end{aligned} \tag{3.41}$$

where $\xi = \sqrt{i\frac{A_2 Pr\alpha^2}{A_3}}$. To determine the constants C_3 and C_4 use of Eqs. (3.27)-(3.28) in Eq. (3.41) gives

$$C_3 = \frac{\alpha\zeta^2 A_4\sqrt{iPrA_2}BesselK[1,\xi]\delta_1 + \zeta^3 A_4\sqrt{A_3}BesselK[0,\xi R^*]\delta_2}{\alpha\zeta^2\sqrt{iPrA_2}\left(BesselI[0,\xi R^*]BesselK[1,\xi] + BesselI[1,\xi]BesselK[0,\xi R^*]\right)}, \tag{3.42}$$

$$C_4 = \frac{\alpha\zeta^2 A_4\sqrt{iPrA_2}BesselI[1,\xi]\delta_1 - \zeta^3 A_4\sqrt{A_3}BesselI[0,\xi R^*]\delta_2}{\alpha\zeta^2\sqrt{iPrA_2}\left(BesselI[0,\xi R^*]BesselK[1,\xi] + BesselI[1,\xi]BesselK[0,\xi R^*]\right)}, \tag{3.43}$$

where

$$\delta_1 = i\left[C_1 I_0(\zeta R^*) + C_2 K_0(\zeta R^*) - i\frac{z}{e^{it}} + \frac{A\alpha^2}{\zeta^2 A_4}\right], \tag{3.44}$$

$$\delta_2 = i\left[C_1 I_1(\zeta) - C_2 K_1(\zeta)\right]. \tag{3.45}$$

3.3 Pressure Calculation

Substitution of solution obtained for $v_z(r,t)$ in equation (3.30) and re-arranging the terms

$$\begin{aligned}\frac{\partial p}{\partial z} =& -A_1\left[i.e^{it}\left(C_1 I_0(\zeta r) + C_2 K_0(\zeta r) + \frac{A\alpha^2}{\zeta^2 A_4}\right)\right] \\ &+ \frac{A_4}{\alpha^2}\left[e^{it}\left(\frac{\zeta^2(I_2(\zeta r) + I_0(\zeta r))}{2}C_1 - \frac{\zeta^2(K_2(\zeta r) + K_0(\zeta r))}{2}C_2\right)\right] \\ &+ \frac{A_4}{\alpha^2}\frac{e^{it}}{r}\left[\zeta I_1(\zeta r)C_1 - \zeta K_1(\zeta r)C_2\right] - \frac{M^2}{\alpha^2}\left[e^{it}\left(C_1 I_0(\zeta r) + C_2 K_0(\zeta r) + \frac{A\alpha^2}{\zeta^2 A_4}\right)\right].\end{aligned} \tag{3.46}$$

The Non-dimensional pressure gradient is defined as

$$\Delta P = \int_0^1 \frac{\partial p}{\partial z} dz, \tag{3.47}$$

and the substitution of (3.46) gives.

$$\Delta P = - A_1 \left[i.e^{it} \left(C_1 I_0(\zeta r) + C_2 K_0(\zeta r) + \frac{A\alpha^2}{\zeta^2 A_4} \right) \right]$$

$$+ \frac{A_4}{\alpha^2} \left[e^{it} \left(\frac{\zeta^2 (I_2(\zeta r) + I_0(\zeta r))}{2} C_1 - \frac{\zeta^2 (K_2(\zeta r) + K_0(\zeta r))}{2} C_2 \right) \right]$$

$$+ \frac{A_4}{\alpha^2} \frac{e^{it}}{r} \left[\zeta I_1(\zeta r) C_1 - \zeta K_1(\zeta r) C_2 \right] - \frac{M^2}{\alpha^2} \left[e^{it} \left(C_1 I_0(\zeta r) + C_2 K_0(\zeta r) + \frac{A\alpha^2}{\zeta^2 A_4} \right) \right]. \tag{3.48}$$

3.4 Results and Discussion

This segment is devoted to analyze the impact of physical parameters on characteristics of temperature and velocity distributions, vorticity and pressure increase for CNTs based nanofluid. The physical parameters are volume fraction of nanoparticles ϕ, Prandtl number Pr, Reynolds number Re_ω, Radiation parameter N_r, magnetic field parameter M, the time t, and the pressure gradient amplitude A. The thermo-physical characteristics of nanofluid are described in Table 3.1.

Table 3.1: The physical characteristics of base fluid and CNTs.

Physical Characteristics	$\rho(kg/m^3)$	$c(J/kgK)$	$k(W/mK)$
Engine oil (Base fluid)	884	1910	0.144
SWCNTs (Nanoparticles)	2600	425	6600
MWCNTs (Nanoparticles)	1600	796	3000

Figures 3.2(a)-(d) presented the influence of certain values of nanoparticles volume fraction on velocity profile. Figures 3.2(a)-(d) show that the velocity field is maximum near the center of cylinder and rapidly decreases with increase of nanoparticle concentration. Figures 3.2(a)-3.2(b) also show that the addition of nanoparticles (both SWCNTs and MWCNTs) in base fluid increases the density of the mixture. As a result, when density of nanofluid is boosted then movement of nanofluid becomes relatively slow as compared to the engine-oil (base fluid) as depicted in Figure 3.2(a)-(b).

Figures 3.3(a)-(d) demonstrate that inclusion of nanoparticles decreases the maximum velocity field of the ordinary fluid. It is observed that the inertial component increase with increase of Womersley number Re_ω. Furthermore, it is also noted that increase of Re_ω give rise in velocity distribution. The Womersley number is the ratio of pulsation to the viscous forces when viscous forces decrease then fluid particles travel faster and thus increases the velocity profile. Figures 3.4(a)-(d) depicts that the maximum of velocity field increases with increase in the value of magnetic field parameter M. Yet there does not hold such observation near to the upper wall. Clearly, an increase intensity of the external magnetic field is obviously intended to increase the velocity of the nanofluid in the middle of the duct. Figures 3.4(a)-(d) often show that the addition of nanoparticles decreases the overall velocity of the base fluid (engine oil). Furthermore, from Figure 3.4(a), it is noted that base fluid have a relatively high velocity field compared to engine oil-SWCNTs ($\phi = 0.2$). Same behavior can be seen in Figure 3.4(b). It is also observed from figures 3.4(a) and 3.4(b) that the magnetic field serve as a resistant force for the fluid flow that eventually reduces the flow rate. In addition, the magnetic field gives rise to the elimination of the annular effect, which is considered a pulsatile flow characteristic.

Figures 3.5(a) and (b) show the effect of the Womersley number Re_ω to examine the velocity field flow for both nanofluid and base fluid. In figure 3.5(a) velocity profile shows the increasing behavior for increasing values of Womersley number close to the surface of the cylinder. It is observed in Figure 3.5(b) that for water based MWCNTs (ϕ= 0.2) the behavior of velocity distribution remains the same but it's values remain low. The decrease in the flow area ends with the rise in dimensionless velocity field as shown in figures 3.6(a) and 3.6(b), where the dimensionless velocity field reduces as nanoparticle concentrations increases. Once again it is observed Figures 3.6(a) and 3.6(b) that engine oil-MWCNT have low velocity field as compare to the engine oil-SWCNT.

Figure 3.7(a)-(d) shows that impact of nanoparticles ϕ on the radial profile of vorticity. According to the vortex definition results presented in Figure 3.7(a)-(d) shows the resemblance and it is found that the effect of the vortices is significantly higher

at extreme level of the domain. We observe that the amplitude of the vortices will be greater if the volume fraction is high for nanofluid. Moreover, the vorticity curves also change their direction along the channel. The vortex graph for SWCNTs and MWCNTs are similar for the same concentration of nanoparticles in base fluid. Figures 3.8 indicates a modification of the pressure gradient in order to maximize the volume of the nanoparticles. It is observed that the pressure gradient at the mean level of the channel is maximum but shows the decreasing behavior. It is also observed that there is a minimum change in the dimensionless pressure gradient for MWCNT as compared to SWCNT.

Figure 3.9(a)-(c) emphasizes the variation in temperature distribution for different values of nanoparticle concentration, pressure gradient amplitude, Hartmann number respectively, for two different nanofluid. Figure 3.9(a) shows the of volume fraction of nanoparticles ϕ on dimensionless temperature profile for engine oil based CNT nanoparticles. It is observed that with an increase of nanoparticles concentration enhance the temperature profile.Furthermore, SWCNT nanoparticles have higher heat transfer rate as compare to the engine oil based MWCNT nanoparticles. Figure 3.9(b) shows the impact of pressure gradient amplitude on the dimensionless temperature for both CNTs. The temperature profile is found to be decreasing with the increase in amplitude of the pressure gradient. Figure 3.9(c) reveals the variance of non-dimensional temperature profile against magnetic parameter M for both nanofluids. We may find that the dimensionless temperature profile increases by introducing the normal magnetic field. Since magnetic field generates the electriccurrent in fluid which generates heat in the fluid, so the magnetic field with thermal radiation improves the enhancement phenomena.

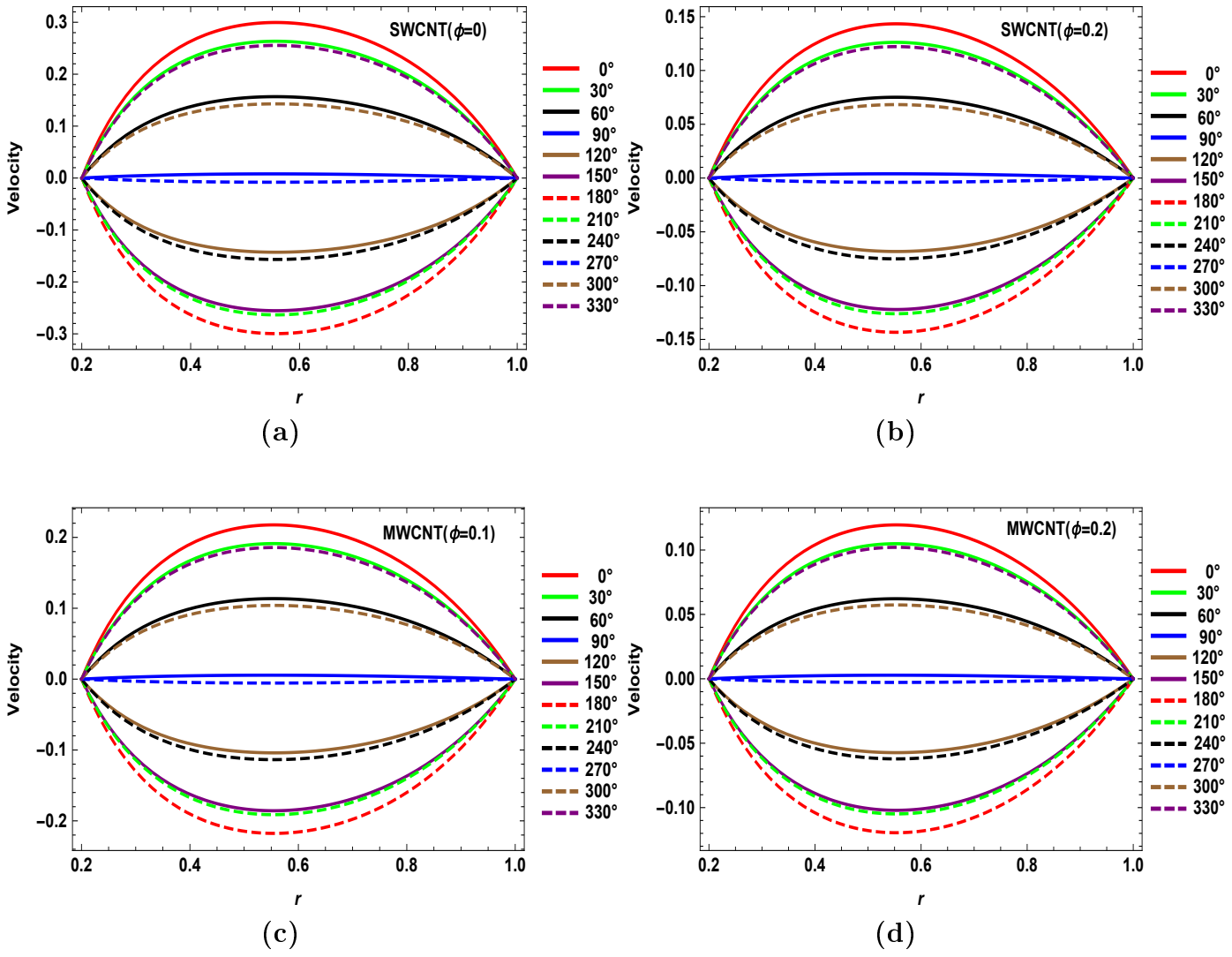

Figure 3.2: Variance in velocity distribution when $M = 5$, $Re_\omega = 1$:

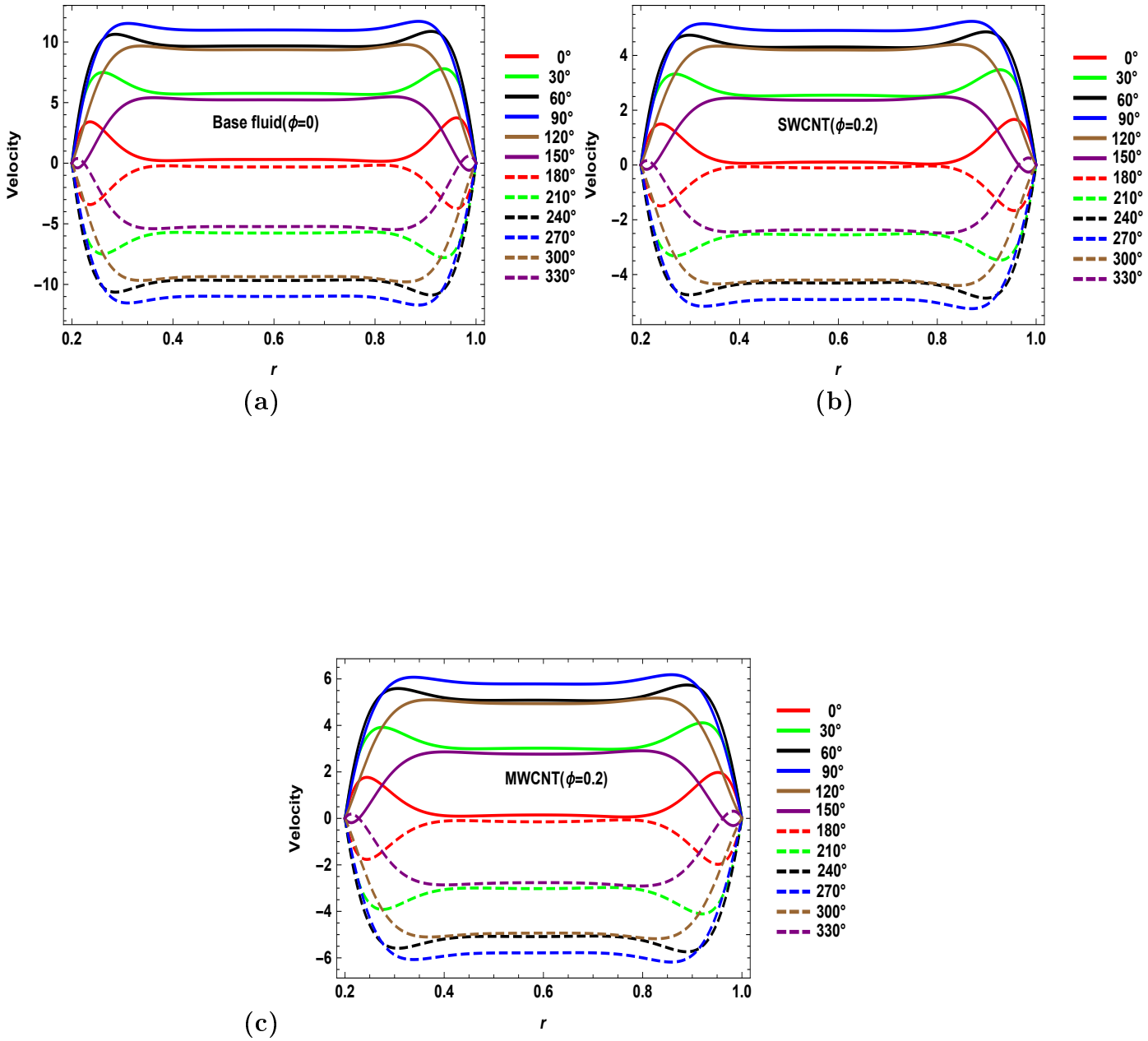

Figure 3.3: Variance in velocity distribution when $M = 5$, $Re_\omega = 900$

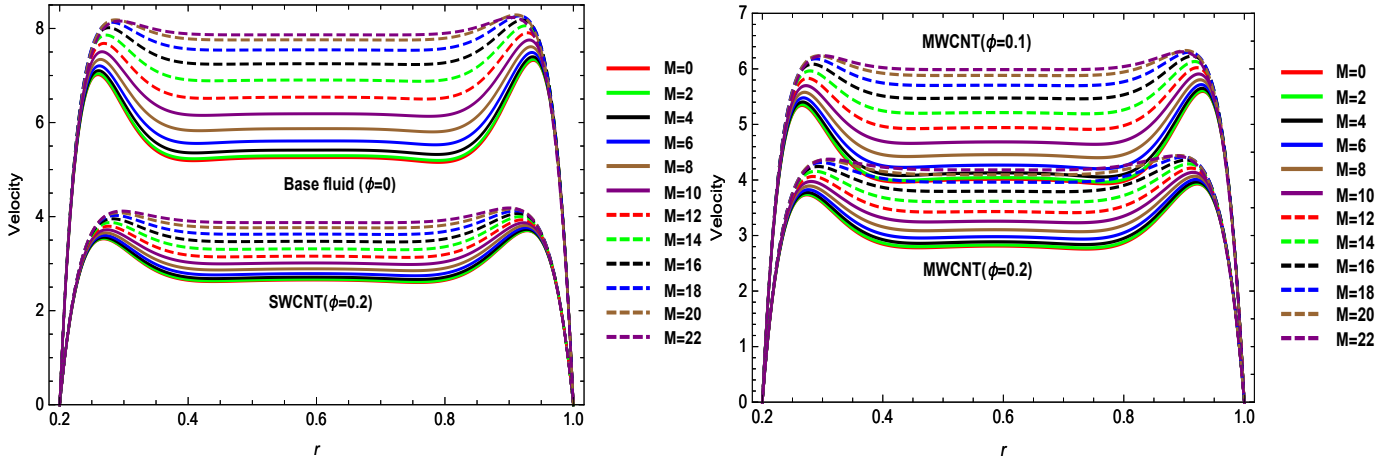

(a) (b)

Figure 3.4: Influence of M on velocity distribution when $Re_\omega = 900$, $t = 30$

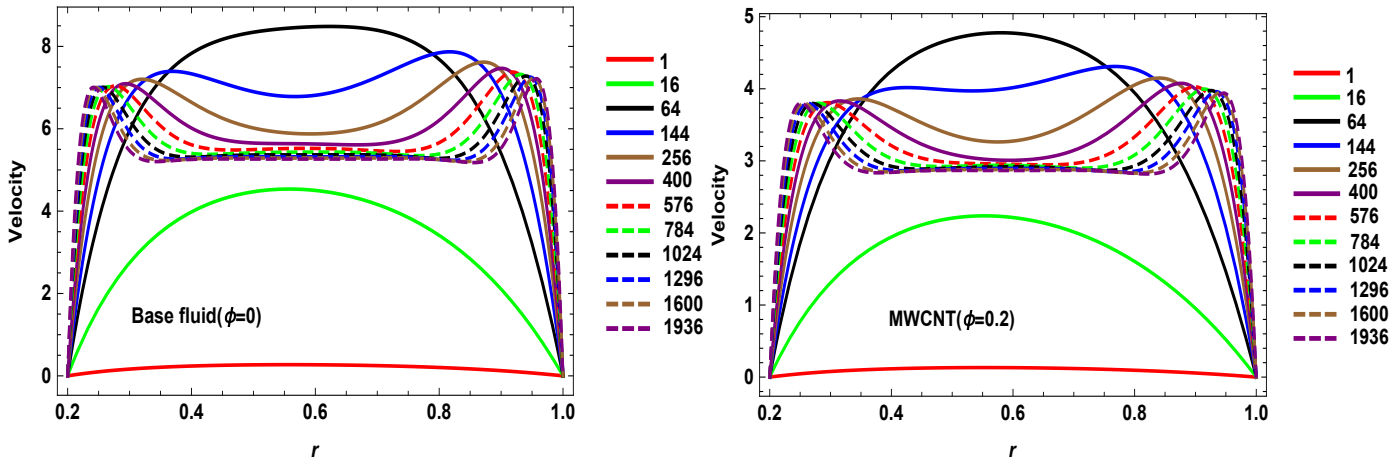

(a) (b)

Figure 3.5: Influence of Re_ω on velocity distribution when $M = 5$, $t = 30$

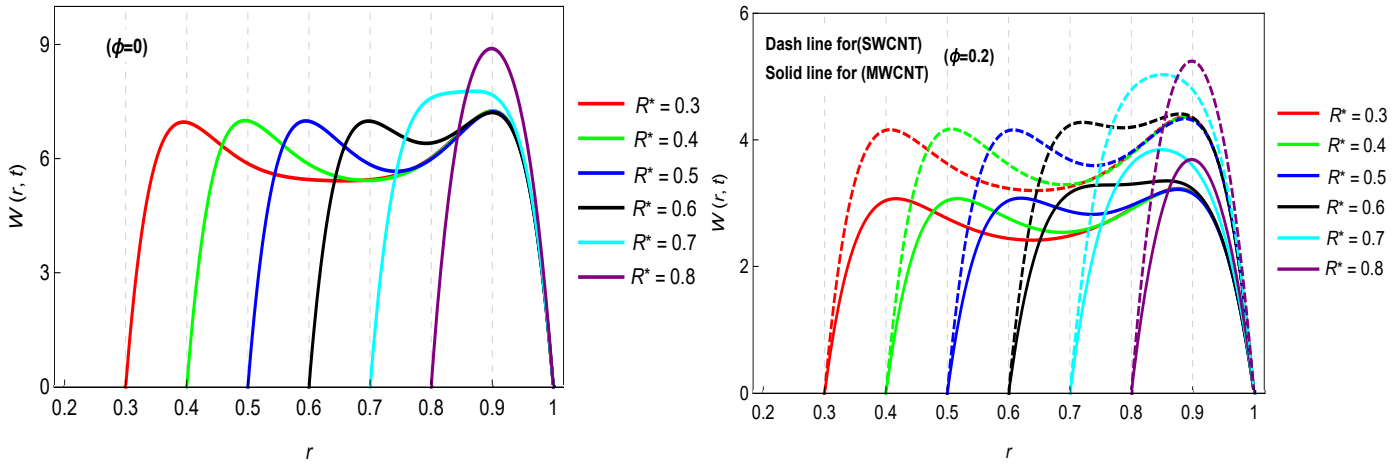

(a) (b)

Figure 3.6: Influence of R^* on velocity distribution when $t = 30$, $M = 5$

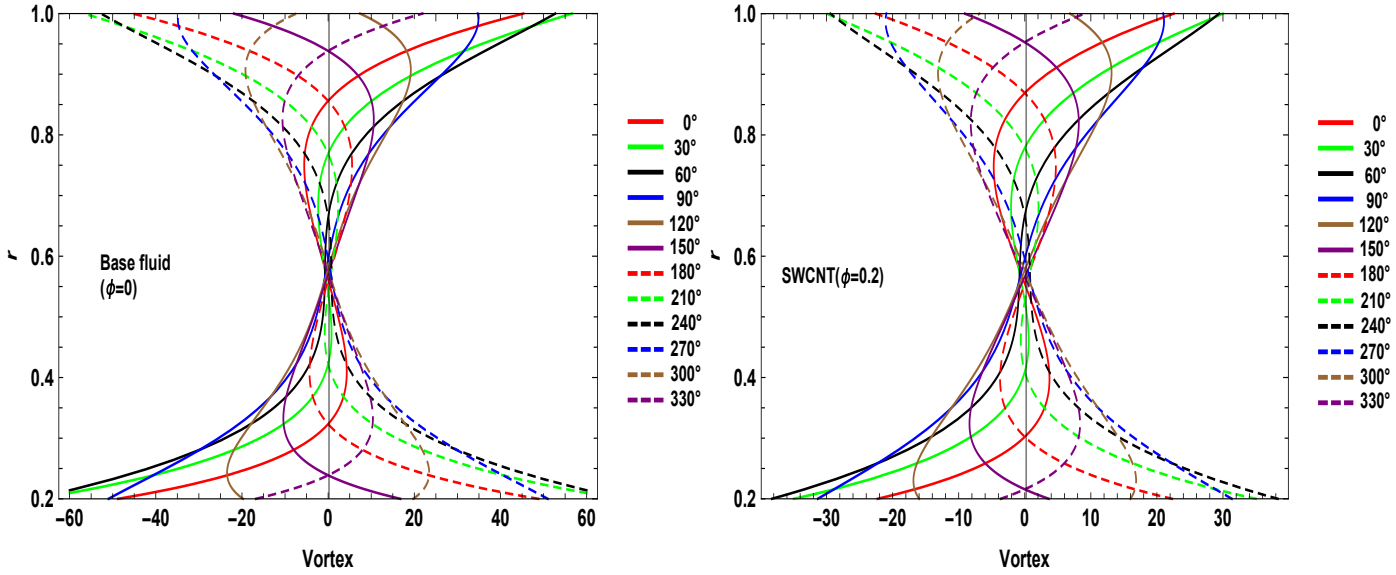

(a) (b)

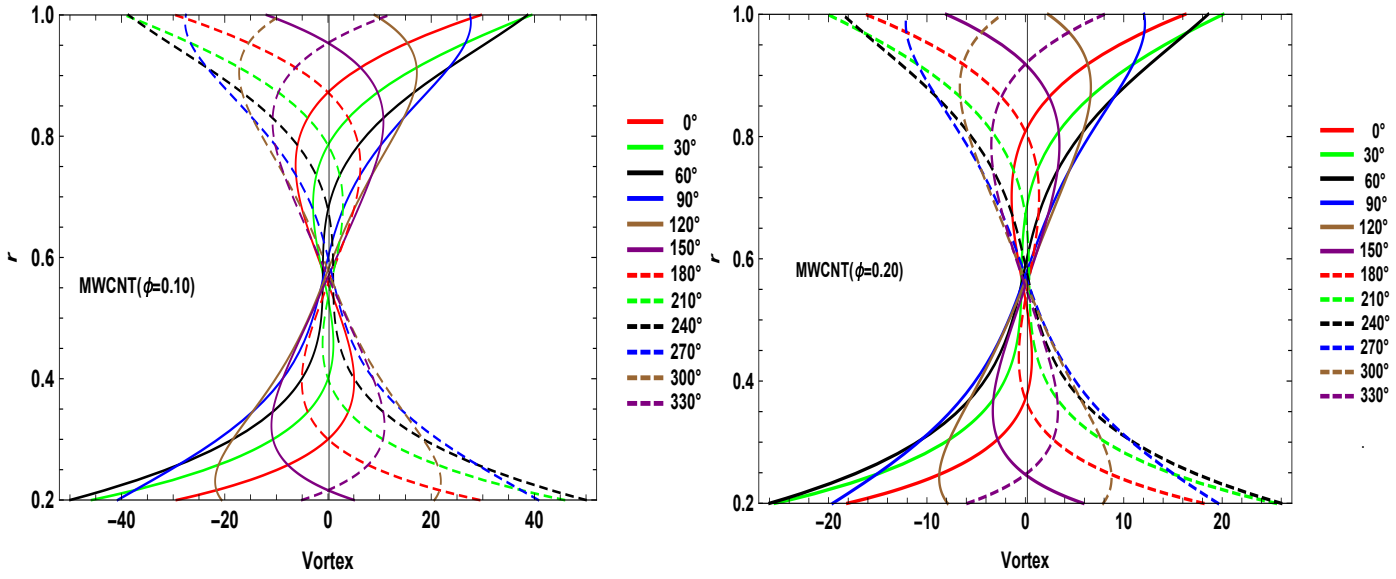

(c) (d)

Figure 3.7: Variation of vortex profile when $Re_\omega = 100$ and $M = 5$

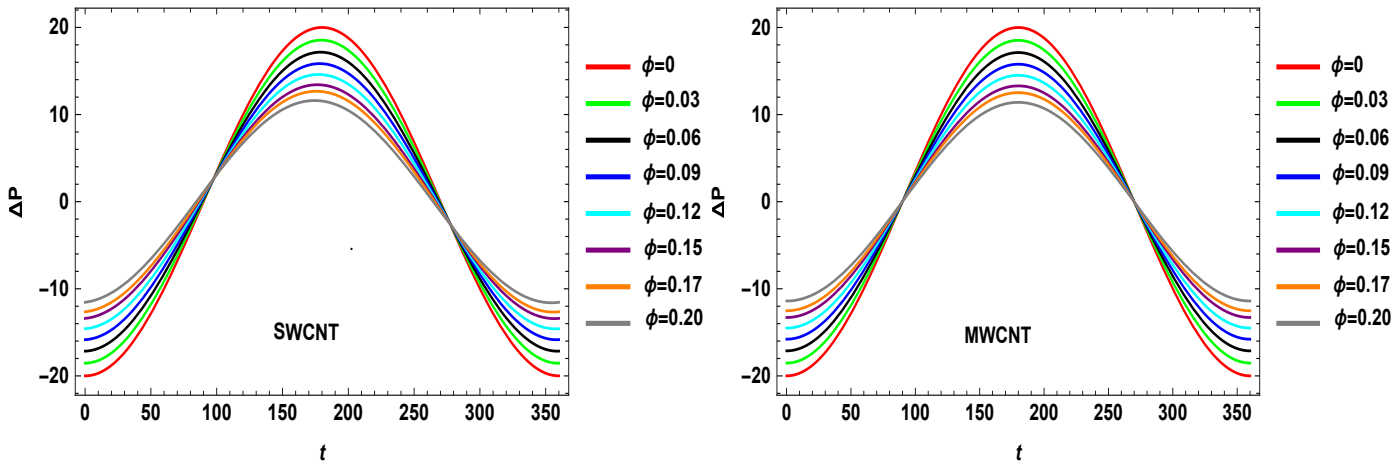

(a) (b)

Figure 3.8: Pressure gradient for (a) SWCNT and (b) MWCNT, when $M = 30$, $Re_\omega = 10$ and $R^* = 0.2$.

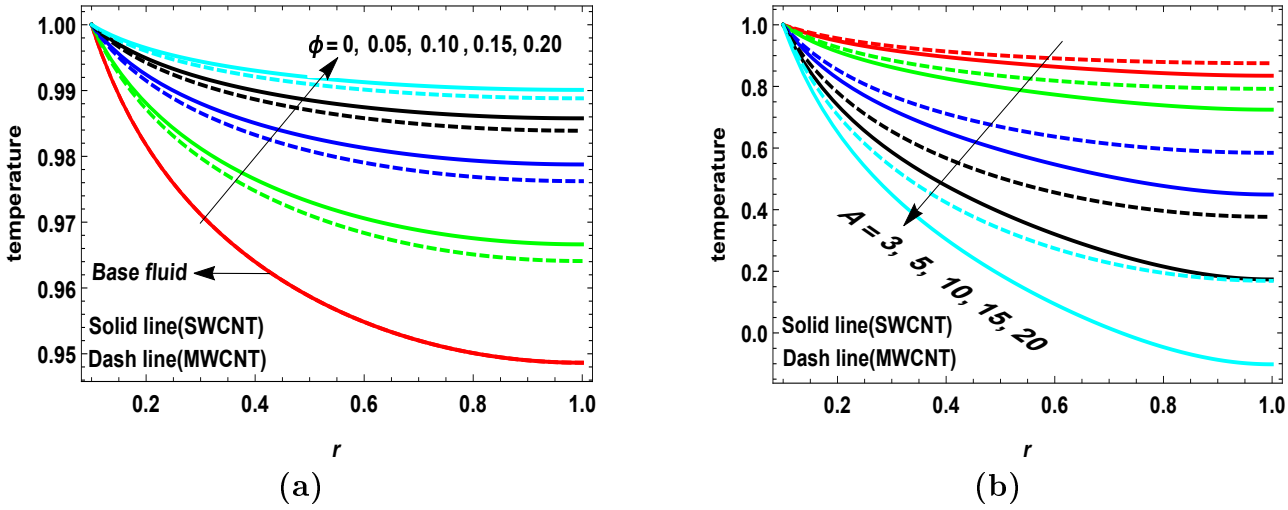

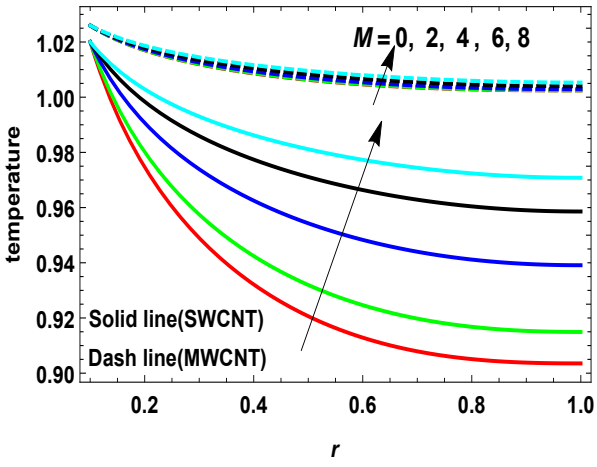

Figure 3.9: Temperature distribution for SWCNTs and MWCNTs (a) Effect of ϕ ;(b) Effect of A ;

Chapter 4

Pulsatile Darcy Flow of Water-Based Thermally Radiative Carbon Nanotubes Between Two Concentric Cylinders

This chapter extends the model presented by Haq et al. [37]. The current investigation analyzes the effects of thermally radiative carbon nanotubes (CNTs) on flow and heat transfer characteristics of viscous fluid in the Darcy type porous medium between two concentric cylinders. Effect of variations in parameters on velocity and temperature profiles are analyzed graphically by using MATHEMATICA. Sections 4.1 deals with the mathematical formulation. Section 4.2 is about the solution of problem and section 4.3 deals with graphical results along with their discussions.

4.1 Formulation of the Problem

Consider the unidirectional MHD flow of viscous fluid moving between two concentric cylinders. The porous space representing the Darcy expression is filled by an incompressible viscous fluid. Nanoparticles are introduced within the viscous fluid to improve the thermal conductivity of the fluid. The nanofluid is produced by inserting CNTs (SWCNTs and MWCNTs) as nanoparticles. The pulsatile pressure gradient is applied in the z-direction to move the fluid within the given channel. The magnetic field B_o is

taken along r-direction. The electric field is taken zero and the induced magnetic field is considered negligible. The nanofluid flow taken under the effect of thermal radiation. As the fluid flow due to the pulsatile pressure, therefore the velocity at cylindrical walls is zero. Further $\vec{V}$=$V(v_r, v_\theta, v_z)$ represents the velocity field. Continuity equation remains same as (2.9) while after including the effects of porous medium and thermal radiation, constitutive equations of momentum and energy are given below

$$\rho_{nf}\left[\frac{\partial \vec{V}}{\partial t} + \vec{V}.\nabla\vec{V}\right] = -\nabla P + \mu_{nf}\nabla^2\vec{V} + \left(\vec{J}\times\vec{B}\right) - \frac{\mu_{nf}}{K}\vec{V}, \tag{4.1}$$

$$(\rho c_p)_{nf}\left[\frac{\partial T}{\partial t} + \vec{V}.\nabla T\right] = \kappa_{nf}\nabla^2 T - \nabla.\vec{q_r}. \tag{4.2}$$

Using Rosseland difusion approximation for thermal radiation the radiative fux q_r is sculpted as

$$\vec{q_r} = -\frac{4\sigma_{sb}}{3a_R}\left[\vec{\nabla}T^4\right], \tag{4.3}$$

$$\nabla.\vec{q_r} = -\frac{4\sigma_{sb}}{3a_R}\left[\nabla^2 T^4\right] = -\frac{4\sigma_{sb}}{3a_R}\left[\frac{1}{r}\frac{\partial T^4}{\partial r} + \frac{\partial^2 T^4}{\partial r^2} + \frac{\partial^2 T^4}{\partial z^2}\right], \tag{4.4}$$

Where, a_R is the mean absorption coefficient and σ_{sb} is Stefan Boltzmann constant. It is supposed that the difference in temperature within the flow is such that T^4 may be represented as the linear combination of temperature. There expanding T^4 by using Taylor series about T_f and considering only linear terms gives us

$$T^4 = 4{T_f}^3 T - 3{T_f}^4. \tag{4.5}$$

Substituting above Equation (4.5) into equation (4.4), we get

$$\nabla.\vec{q_r} = -\frac{16\sigma_{sb}{T_f}^3}{3a_R}\left[\frac{1}{r}\frac{\partial T}{\partial r} + \frac{\partial^2 T}{\partial r^2} + \frac{\partial^2 T}{\partial z^2}\right], \tag{4.6}$$

In cylindrical coordinates system, equations (4.1) and (4.2) will become

$$\rho_{nf}\left[\frac{\partial v_r}{\partial t}+v_r\frac{\partial v_r}{\partial r}+v_z\frac{\partial v_r}{\partial z}\right] = -\frac{\partial p}{\partial r}+\mu_{nf}\left[\frac{1}{r}\frac{\partial v_r}{\partial r}+\frac{\partial^2 v_r}{\partial r^2}+\frac{\partial^2 v_r}{\partial z^2}-\frac{v_r}{r^2}\right]-\frac{\mu_{nf}}{K}v_r, \tag{4.7}$$

$$\rho_{nf}\left[\frac{\partial v_z}{\partial t}+v_r\frac{\partial v_z}{\partial r}+v_z\frac{\partial v_z}{\partial z}\right] = -\frac{\partial p}{\partial z}+\mu_{nf}\left[\frac{1}{r}\frac{\partial v_z}{\partial r}+\frac{\partial^2 v_z}{\partial r^2}+\frac{\partial^2 v_z}{\partial z^2}\right]-\sigma_f {B_o}^2 v_z-\frac{\mu_{nf}}{K}v_z, \tag{4.8}$$

$$(\rho c_p)_{nf}\left[\frac{\partial T}{\partial t}+v_r\frac{\partial T}{\partial r}+v_z\frac{\partial T}{\partial z}\right] = \kappa_{nf}\left[\frac{1}{r}\frac{\partial T}{\partial r}+\frac{\partial^2 T}{\partial r^2}+\frac{\partial^2 T}{\partial z^2}\right]+\frac{16\sigma_{sb}{T_f}^3}{3a_R}\left[\frac{1}{r}\frac{\partial T}{\partial r}+\frac{\partial^2 T}{\partial r^2}+\frac{\partial^2 T}{\partial z^2}\right]. \tag{4.9}$$

Substitute equations (3.6)-(3.9) into Equations (4.7), (4.8) and (4.9) we obtain

$$\rho_f\left[(1-\phi)+\left(\frac{\rho_{CNT}}{\rho_f}\right)\phi\right]\left[\frac{\partial v_r}{\partial t}+v_r\frac{\partial v_r}{\partial r}+v_z\frac{\partial v_r}{\partial z}\right] = -\frac{\partial p}{\partial r}+\frac{\mu_f}{(1-\phi)^{2.5}}\left[\frac{1}{r}\frac{\partial v_r}{\partial r}+\frac{\partial^2 v_r}{\partial r^2}+\frac{\partial^2 v_r}{\partial z^2}-\frac{v_r}{r^2}\right]-\frac{\mu_{nf}}{K}v_r, \tag{4.10}$$

$$\rho_f\left[(1-\phi)+\left(\frac{\rho_{CNT}}{\rho_f}\right)\phi\right]\left[\frac{\partial v_z}{\partial t}+v_r\frac{\partial v_z}{\partial r}+v_z\frac{\partial v_z}{\partial z}\right] = -\frac{\partial p}{\partial z}+\frac{\mu_f}{(1-\phi)^{2.5}}\left[\frac{1}{r}\frac{\partial v_z}{\partial r}+\frac{\partial^2 v_z}{\partial r^2}+\frac{\partial^2 v_z}{\partial z^2}\right]-\sigma_f B_o^2 v_z-\frac{\mu_{nf}}{K}v_z, \tag{4.11}$$

$$(\rho c_p)_f\left[(1-\phi)+\left(\frac{(\rho c_p)_{CNT}}{(\rho c_p)_f}\right)\phi\right]\left[\frac{\partial T}{\partial t}+v_r\frac{\partial T}{\partial r}+v_z\frac{\partial T}{\partial z}\right] = \kappa_{nf}\left[\frac{1}{r}\frac{\partial T}{\partial r}+\frac{\partial^2 T}{\partial r^2}+\frac{\partial^2 T}{\partial z^2}\right]+\frac{16\sigma_{sb}{T_f}^3}{3a_R}\left[\frac{1}{r}\frac{\partial T}{\partial r}+\frac{\partial^2 T}{\partial r^2}+\frac{\partial^2 T}{\partial z^2}\right]. \tag{4.12}$$

Now we transform the above dimensional flow equations (4.10)-(4.12) into non-dimensional form using variables v_r, v_z, r, z, t, p and T defined in equation (3.16)

$$\begin{aligned}
&\left[(1-\phi)+\left(\frac{\rho_{CNT}}{\rho_f}\right)\phi\right]\left[\frac{\partial v_r}{\partial t}+v_r\frac{\partial v_r}{\partial r}+v_z\frac{\partial v_r}{\partial z}\right]\\
&\quad=-\frac{\partial p}{\partial r}+\frac{\mu_f}{(1-\phi)^{2.5}\,\omega {R_e}^2\rho_f}\left[\frac{1}{r}\frac{\partial v_r}{\partial r}+\frac{\partial^2 v_r}{\partial r^2}+\frac{\partial^2 v_r}{\partial z^2}-\frac{v_r}{r^2}\right]\\
&\qquad-\frac{\mu_f}{(1-\phi)^{2.5}\,\omega\rho_f K}v_r, \qquad (4.13)
\end{aligned}$$

$$\begin{aligned}
&\left[(1-\phi)+\left(\frac{\rho_{CNT}}{\rho_f}\right)\phi\right]\left[\frac{\partial v_z}{\partial t}+v_r\frac{\partial v_z}{\partial r}+v_z\frac{\partial v_z}{\partial z}\right]\\
&\quad=-\frac{\partial p}{\partial z}+\frac{\mu_f}{(1-\phi)^{2.5}\,\omega {R_e}^2\rho_f}\left[\frac{1}{r}\frac{\partial v_z}{\partial r}+\frac{\partial^2 v_z}{\partial r^2}+\frac{\partial^2 v_z}{\partial z^2}\right]\\
&\qquad-\frac{\sigma_f B_o^2}{\omega\rho_f}v_z-\frac{\mu_f}{(1-\phi)^{2.5}\,\omega\rho_f K}v_z, \qquad (4.14)
\end{aligned}$$

$$\begin{aligned}
&\left[(1-\phi)+\left(\frac{(\rho c_p)_{CNT}}{(\,\rho c_p)_f}\right)\phi\right]\left[\frac{\partial T}{\partial t}+v_r\frac{\partial T}{\partial r}+v_z\frac{\partial T}{\partial z}\right]\\
&\quad=\frac{\kappa_{nf}}{\omega {R_e}^2\,(\rho c_p)_f}\left[\frac{1}{r}\frac{\partial T}{\partial r}+\frac{\partial^2 T}{\partial r^2}+\frac{\partial^2 T}{\partial z^2}\right]\\
&\qquad+\frac{16\sigma_{sb}{T_f}^3}{3a_R\omega {R_e}^2\,(\rho c_p)_f}\left[\frac{1}{r}\frac{\partial T}{\partial r}+\frac{\partial^2 T}{\partial r^2}+\frac{\partial^2 T}{\partial z^2}\right]. \qquad (4.15)
\end{aligned}$$

After simplifying the above equations (4.13)-(4.15) we obtain

$$A_1\left[\frac{\partial v_r}{\partial t}+v_r\frac{\partial v_r}{\partial r}+v_z\frac{\partial v_r}{\partial z}\right] = -\frac{\partial p}{\partial r}+\frac{A_4}{Re_\omega}\left[\frac{1}{r}\frac{\partial v_r}{\partial r}+\frac{\partial^2 v_r}{\partial r^2}+\frac{\partial^2 v_r}{\partial z^2}-\frac{v_r}{r^2}\right]-\frac{A_4}{Re_\omega.D_a}v_r, \tag{4.16}$$

$$A_1\left[\frac{\partial v_z}{\partial t}+v_r\frac{\partial v_z}{\partial r}+v_z\frac{\partial v_z}{\partial z}\right] = -\frac{\partial p}{\partial z}+\frac{A_4}{Re_\omega}\left[\frac{1}{r}\frac{\partial v_z}{\partial r}+\frac{\partial^2 v_z}{\partial r^2}+\frac{\partial^2 v_z}{\partial z^2}\right]-\frac{M^2}{Re_\omega}v_z-\frac{A_4}{Re_\omega.D_a}v_z, \tag{4.17}$$

$$A_2\left[\frac{\partial T}{\partial t}+v_r\frac{\partial T}{\partial r}+v_z\frac{\partial T}{\partial z}\right] = \left[\frac{A_3}{Pr.Re_\omega}+\frac{N_r}{Re_\omega}\right]\left[\frac{1}{r}\frac{\partial T}{\partial r}+\frac{\partial^2 T}{\partial r^2}+\frac{\partial^2 T}{\partial z^2}\right]. \tag{4.18}$$

The dimensionless parameters appearing in Eqs. (4.16)-(4.18) are defined as

$$Pr=\frac{\mu_f(c_p)_f}{\kappa_f}, \qquad M=R_eB_o\sqrt{\frac{\sigma_f}{\mu_{\mathrm{f}}}}, \qquad Re_\omega=\alpha^2=\frac{\omega R_e^2}{\nu_f},$$
$$D_a=\frac{K}{R_e^2}, \qquad N_r=\frac{16\sigma_{sb}{T_f}^3}{3a_R\nu_f\left(\rho c_p\right)_f}. \tag{4.19}$$

Assume the flow is fully developed and the velocity field is of the form

$$\vec{V}=\left[0,0,v_z(r,z,t)\right]. \tag{4.20}$$

The flow field defined in equation (4.20) identically satisfies the continuity equation (2.9) and the eqs. (4.16)-(4.18) can be rewritten as

$$A_1\frac{\partial v_z}{\partial t}=-\frac{\partial p}{\partial z}+\frac{A_4}{Re_\omega}\left[\frac{\partial^2 v_z}{\partial r^2}+\frac{1}{r}\frac{\partial v_z}{\partial r}\right]-\frac{M^2}{Re_\omega}v_z-\frac{A_4}{Re_\omega.D_a}v_z, \tag{4.21}$$

$$A_2\left[\frac{\partial T}{\partial t}+v_z\frac{\partial T}{\partial z}\right]=\left[\frac{A_3}{Pr.Re_\omega}+\frac{N_r}{Re_\omega}\right]\left[\frac{\partial^2 T}{\partial r^2}+\frac{1}{r}\frac{\partial T}{\partial r}+\frac{\partial^2 T}{\partial z^2}\right]. \tag{4.22}$$

In case of axis-symmetric flow equations (4.21) and (4.22) becomes

$$A_1\frac{\partial v_z}{\partial t}=-\frac{\partial p}{\partial z}+\frac{A_4}{\alpha^2}\left[\frac{\partial^2 v_z}{\partial r^2}+\frac{1}{r}\frac{\partial v_z}{\partial r}\right]-\frac{M^2}{\alpha^2}v_z-\frac{A_4}{\alpha^2.D_a}v_z, \tag{4.23}$$

$$A_2\left[\frac{\partial T}{\partial t}+v_z\frac{\partial T}{\partial z}\right]=\left[\frac{A_3}{Pr.\alpha^2}+\frac{N_r}{\alpha^2}\right]\left[\frac{\partial^2 T}{\partial r^2}+\frac{1}{r}\frac{\partial T}{\partial r}+\frac{\partial^2 T}{\partial z^2}\right]. \tag{4.24}$$

4.2 Solution of the Problem

The problem considered in this study deals with the pulsatile flow and heat transfer, therefore periodic pressure gradient can be expressed as

$$\frac{\partial P}{\partial z} = -ACos(\omega t) = Real(-Ae^{i\omega t}). \tag{4.25}$$

The velocity profile solution can be described as

$$v_z(r,t) = Real\left[f(r)e^{it}\right]. \tag{4.26}$$

In view of equations (4.25) and (4.26), we have from equation (4.23)

$$\frac{d^2f(r)}{dr^2} + \frac{1}{r}\frac{df(r)}{dr} - \left[\frac{(M^2 + i\alpha^2 A_1)}{A_4} + \frac{1}{D_a}\right] f(r) = -\frac{A\alpha^2}{A_4}. \tag{4.27}$$

The solution to linear second order ODE (4.27) is in the form of Bessel's functions

$$f(r) = C_1 I_0(\eta r) + C_2 K_0(\eta r) + \frac{A\alpha^2}{\eta^2 A_4}, \tag{4.28}$$

where I_0 and K_0 are zeroth order Bessel's function of the first kind and the second kind respectively. $\eta = \sqrt{\frac{(M^2+i\alpha^2 A_1)}{A_4} + \frac{1}{D_a}}$. Equation (4.26) together with (4.28) yields

$$v_z(r,t) = Real\left[C_1 I_0(\eta r) + C_2 K_0(\eta r) + \frac{A\alpha^2}{\eta^2 A_4}\right] e^{it} \tag{4.29}$$

To determine the constants C_1 and C_2 Eqs. (3.27)-(3.28) are substituted in Eq. (4.29). After simplification

$$C_1 = \frac{-\alpha^2 BesselK[0,\eta]A + \alpha^2 BesselK[0,\eta R^*]A}{\eta^2 A_4\left(BesselI[0,\eta R^*]BesselK[0,\eta] - BesselI[0,\eta]BesselK[0,\eta R^*]\right)}, \tag{4.30}$$

$$C_2 = \frac{\alpha^2 BesselI[0,\eta]A - \alpha^2 BesselI[0,\eta R^*]A}{\eta^2 A_4\left(BesselI[0,\eta R^*]BesselK[0,\eta] - BesselI[0,\eta]BesselK[0,\eta R^*]\right)}. \tag{4.31}$$

In order to find the analytical solution of the Eq. (4.24), the solution for the temperature profile is assumed as

$$T(r,z,t) = Real\left[-\gamma^{'}z + \gamma^{'}g(r)e^{it} + 1\right], \tag{4.32}$$

where $\gamma^{'} = \frac{Re}{L}$. Eq. (4.24) in light of the above takes the form

$$\frac{d^2g(r)}{dr^2} + \frac{1}{r}\frac{dg(r)}{dr} - i\frac{A_2Pr\alpha^2}{A_3 + PrN_r}g(r) = \frac{A_2Pr\alpha^2}{A_3 + PrN_r}f(r). \tag{4.33}$$

The solution of Eq. (4.33) is

$$\begin{aligned} T(r,z,t) = Real[-\gamma^{'}z + \gamma^{'}[-iC_1I_0(\eta r) - iC_2K_0(\eta r) + C_3I_0(\xi r) \\ + C_4K_0(\xi r) - i\frac{A\alpha^2}{\eta^2 A_4}]e^{it} + 1], \end{aligned} \tag{4.34}$$

where $\xi = \sqrt{i\frac{A_2Pr\alpha^2}{A_3+PrN_r}}$. To determine the constants C_3 and C_4 use of Eqs. (3.27)-(3.28) in Eq. (4.34) gives

$$C_3 = \frac{\alpha\eta^2A_4\sqrt{iPrA_2}BesselK[1,\xi]\beta_1 + \eta^3A_4\sqrt{A_3 + PrN_r}BesselK[0,\xi R^*]\beta_2}{\alpha\eta^2\sqrt{iPrA_2}\left(BesselI[0,\xi R^*]BesselK[1,\xi] + BesselI[1,\xi]BesselK[0,\xi R^*]\right)A_4}, \tag{4.35}$$

$$C_4 = \frac{\alpha\eta^2A_4\sqrt{iPrA_2}BesselI[1,\xi]\beta_1 - \eta^3A_4\sqrt{A_3 + PrN_r}BesselI[0,\xi R^*]\beta_2}{\alpha\eta^2\sqrt{iPrA_2}\left(BesselI[0,\xi R^*]BesselK[1,\xi] + BesselI[1,\xi]BesselK[0,\xi R^*]\right)A_4}, \tag{4.36}$$

$$\beta_1 = \left[\frac{z}{e^{it}} + i\frac{A\alpha^2}{\eta^2A_4} + iC_1I_0(\eta R^*) + iC_2K_0(\eta R^*)\right], \tag{4.37}$$

$$\beta_2 = \left[iC_1I_1(\eta) - iC_2K_1(\eta)\right]. \tag{4.38}$$

4.3 Pressure Calculation

To calculate the pressure gradient, Equation (4.23) can be written as

$$\frac{\partial p}{\partial z} = -A_1\frac{\partial v_z}{\partial t} + \frac{A_4}{\alpha^2}\left[\frac{\partial^2 v_z}{\partial r^2} + \frac{1}{r}\frac{\partial v_z}{\partial r}\right] - \frac{M^2}{\alpha^2}v_z - \frac{A_4}{\alpha^2.D_a}v_z \tag{4.39}$$

Equation (4.39) together with Eq. (4.29) becomes

$$\frac{\partial p}{\partial z} = -A_1 \left[i.e^{it} \left(C_1 I_0(\eta r) + C_2 K_0(\eta r) + \frac{A\alpha^2}{\eta^2 A_4} \right) \right]$$

$$+ \frac{A_4}{\alpha^2} \left[e^{it} \left(\frac{\eta^2 (I_2(\eta r) + I_0(\eta r))}{2} C_1 - \frac{\eta^2 (K_2(\eta r) + K_0(\eta r))}{2} C_2 \right) \right]$$

$$+ \frac{A_4}{\alpha^2} \frac{e^{it}}{r} \left[\eta I_1(\eta r) C_1 - \eta K_1(\eta r) C_2 \right] - \frac{M^2}{\alpha^2} \left[e^{it} \left(C_1 I_0(\eta r) + C_2 K_0(\eta r) + \frac{A\alpha^2}{\eta^2 A_4} \right) \right]$$

$$- \frac{A_4}{\alpha^2 . D_a} \left[e^{it} \left(C_1 I_0(\eta r) + C_2 K_0(\eta r) + \frac{A\alpha^2}{\eta^2 A_4} \right) \right]. \tag{4.40}$$

The dimensionless pressure rise is define as

$$\Delta P = \int_0^1 \frac{\partial p}{\partial z} dz \tag{4.41}$$

$$\Delta P = -A_1 \left[i.e^{it} \left(C_1 I_0(\eta r) + C_2 K_0(\eta r) + \frac{A\alpha^2}{\eta^2 A_4} \right) \right]$$

$$+ \frac{A_4}{\alpha^2} \left[e^{it} \left(\frac{\eta^2 (I_2(\eta r) + I_0(\eta r))}{2} C_1 - \frac{\eta^2 (K_2(\eta r) + K_0(\eta r))}{2} C_2 \right) \right]$$

$$+ \frac{A_4}{\alpha^2} \frac{e^{it}}{r} \left[\eta I_1(\eta r) C_1 - \eta K_1(\eta r) C_2 \right] - \frac{M^2}{\alpha^2} \left[e^{it} \left(C_1 I_0(\eta r) + C_2 K_0(\eta r) + \frac{A\alpha^2}{\eta^2 A_4} \right) \right]$$

$$- \frac{A_4}{\alpha^2 . D_a} \left[e^{it} \left(C_1 I_0(\eta r) + C_2 K_0(\eta r) + \frac{A\alpha^2}{\eta^2 A_4} \right) \right]. \tag{4.42}$$

4.4 Results and Discussion

This segment is devoted to analyze the impact of physical parameters on characteristics of temperature and velocity distributions, vorticity and pressure increase for CNTs

based nanofluid. The physical parameters are volume fraction of nanoparticles ϕ, Prandtl number Pr, Reynolds number Re_ω, Radiation parameter N_r, magnetic field parameter M, Darcy parameter D_a, the pressure gradient amplitude A and the time t. The values of various parameters considered are $Pr = 6.2$, $r^* = 0.1$ and $z = 3$ while other parameters are varied over a range and are mentioned in the caption of the figures. The thermo-physical characteristics of nanofluid are described in Table 1.

Table 4.1: The physical characteristics of nanoparticles and base fluid [29].

Physical Characteristics	$\rho(kg/m^3)$	$C(J/kgK)$	$k(W/mK)$
SWCNTs (Nano Particle)	2600	425	6600
MWCNTs (Nano Particle)	1600	796	3000
Water (Base Fluid)	997.1	4179	0.613

Figures (4.1)-(4.6) are plotted to see how physical parameters affect the velocity profile for CNTs based nanofluid. In Figures 4.1(a)–4.1(d) effects of variation in the solid volume fraction of nanoparticle ϕ on the velocity profiles are presented. Each plotted graph shows that the enhancement of solid volume fraction of nanoparticles leads to the velocity profile attains the highest amplitude at the mean level of the duct and shows a parabolic curve which swiftly decreases with raise in nanoparticles concentration In Figure 4.1(a), one can notice that there is a higher and significant change in the velocity distribution for $\phi = 0$ as compared to the nonzero values of solid volume fraction of nanoparticles ϕ. When comparison is made between velocity profile of SWCNT and MWCNT for same concentration of nanoparticles, we notice that the peak velocity for SWCNT is higher as compared to MWCNT. Figures 4.2(a)-4.2(d) demonstrate that the highest velocity in pulsatile flow is found close to the walls of the cylinders with rapid vibrations due to the annular effect. These annular effects increase with increase in Womersley number. In this case again we have lower velocity for the case of MWCNTs. Overall presence of nanoparticles decrease the velocity profile for pulsatile flow.

Figures 4.3(a)-4.3(d) show that the velocity deviate slightly from sinusoidal mean velocity and gives rise to more significant annular effect. Radial velocity close to the cylinder wall becomes steeper and friction force improves with increase in Womersley number. Figure 4.4(a)-(d) is plotted to compare the effects of Hartmann number. The presence of magnetic field for smaller values of Womersley number develops the uniform flow field about the center of cylinder. In this case, the effects of SWCNTs and MWCNTs on velocity field are almost similar. Moreover, the velocity distribution for $M = 10$ reaches a maximum range at the mean level and follows a parabolic curve (see Figure 4.4). Figure 4.4(a)-(d) also showed that the maximum velocity of the base fluid is reduced due to addition of nanoparticles. In addition, the magnetic field and low values of Womersley number give rise to the termination of the annular effect which is perceived to be a response of pulsatile flow.

Figures 4.5(a)-4.5(b) are plotted to show the effects of Hartmann number on the fluid flow. It also compares the two different nanofluids behavior under the influence of magnetic field. The significant difference in the velocity fields is visible for the presence and absence of magnetic field. The velocity field increases with the increase in values of magnetic parameter. In this case pulsatile effects are also visible which were earlier missing for the smaller values of Womersley number. When SWCNTs and MWCNTs are compared, generally it is noticed that for MWCNTs velocity variation is more pronounced against magnetic parameter as compared to SWCNTs. Figures 4.6(a)-4.6(b) show the effects of the Womersley number Re_ω on the flow velocity for nanofluid and base fluid. Womersley number appears to be the controlling parameter in determining the nature of pulsatile flow. Smaller values of Womersley number means little or no effects of pulsatile motion. However, for larger values a significant variation in velocity profile can be noticed. It changes from being a symmetric flow about the mean position to a pulsative shape. The velocity almost maintain a constant value for $r = 0.4$ to $r = 0.8$. It is observed in Figure 4.6(b) that for water based MWCNTs (ϕ= 0.2) the behavior of velocity distribution remains the same but it's values remain low. Figures 4.8(a)-4.8(b) show the unsteady velocity distribution at $t = 30$ for different values of

R^*. It is observed that the velocity curve is changing it's shape as the values of R^* are changed. The velocity curve shape is changing from spanned pulsating shape to steep parabolic shape. In pulsating shape it has two peaks of equal height. When comparison is made between SWCNTs and MWCNTs, we notice that the general behaviour remains unaffected by choice of nanoparticles. However, the velocity for the case of MWCNTs remains to be on lower side. It is observed that the flow area constructs the envelope set for different radius values and he velocity distribution reaches the highest position with respect to increasing radius values.

Figures 4.7(a)-4.7(d) depict the velocity variance for different values of Darcy number. Since the drag force is inversely proportional to the Darcy number, known as Darcian force (view last term of Equation (4.23), that is, $\frac{-w}{D_a}$). Therefore, w increases with the increase of D_a. In addition, with increase in D_a, the velocity distribution attains the highest amplitude at the mean position and maintains a parabolic curve. The SWCNTs have a pronounced effect on velocity as compared to the MWCNTs. Figures 4.9(a)-4.9(d) show the volume fraction effects on the vorticity distribution. We observe that the amplitude of the vortices will be greater if the volume fraction is high for nanofluid. It is also important to realize that for certain processes the vorticity takes negative values based on the existence of a return flow for the different values of parameters. Vorticity effects are more dominant in the absence of nanoparticles (see Figures 4.9(a)-4.9(d)). It appears to be zero at mean position and increase as move away from mean position in either direction. Moreover, the vorticity curves also change their direction along the channel. The vortex graph for SWCNTs and MWCNTs are similar for the same concentration of nanoparticles in base fluid. Figures 4.10(a)-4.10(b) indicate a modification of the pressure gradient in order to maximize the volume of the nanoparticles. It's also observed that the pressure at $t = 180^o$ is maximum but obtain the decreasing behaviour. Although, the pressure gradient at $t = 0^o$ and $t = 360^o$ is minimal but it increases with the increase in nanoparticles concentration.

Figures 4.11(a-d) are plotted to see how physical parameters affect the tempera-

ture profile for both CNTs. Figures 4.11(a-d) show the influences of different physical parameters on dimensionless temperature distribution. Generally, temperature profile decreases with the raising values of r for both SWCNTs and MWCNTs. However, when nanoparticles concentration is increased the temperature profile raises. Furthermore, the temperature profile for SWCNTs is slightly higher as compared to MWCNTs. The maximum values of nanoparticles concentration is kept at 0.2 to make sure that the nature of the fluid does not change. Figure 4.11(b) shows the impact of pressure gradient amplitude on the dimensionless temperature for both CNTs. The temperature profile is found to be decreasing with the increase in amplitude of the pressure gradient. In this case the gap between the corresponding temperature curves for both CNTs increases across the radius of cylinder. Which suggests that SWCNTs and MWCNTs behave differently under the applied stress. Overall, the temperature profile is higher for MWCNTs which is opposite to what is observed in figure 4.11(a). Figure 4.11(c) shows that the dimensionless temperature distribution decreases with the increase in darcy number. It is also found that the dimensionless temperature distribution is slightly lower for SWCNTs as compared to MWCNTs. Figure 4.11(d) shows the variation of temperature profile against thermal radiation parameter. Temperature profile increases with the increase in thermal radiation parameter. It is noticed that the temperature profile for SWCNTs is slightly lower than MWCNTs.

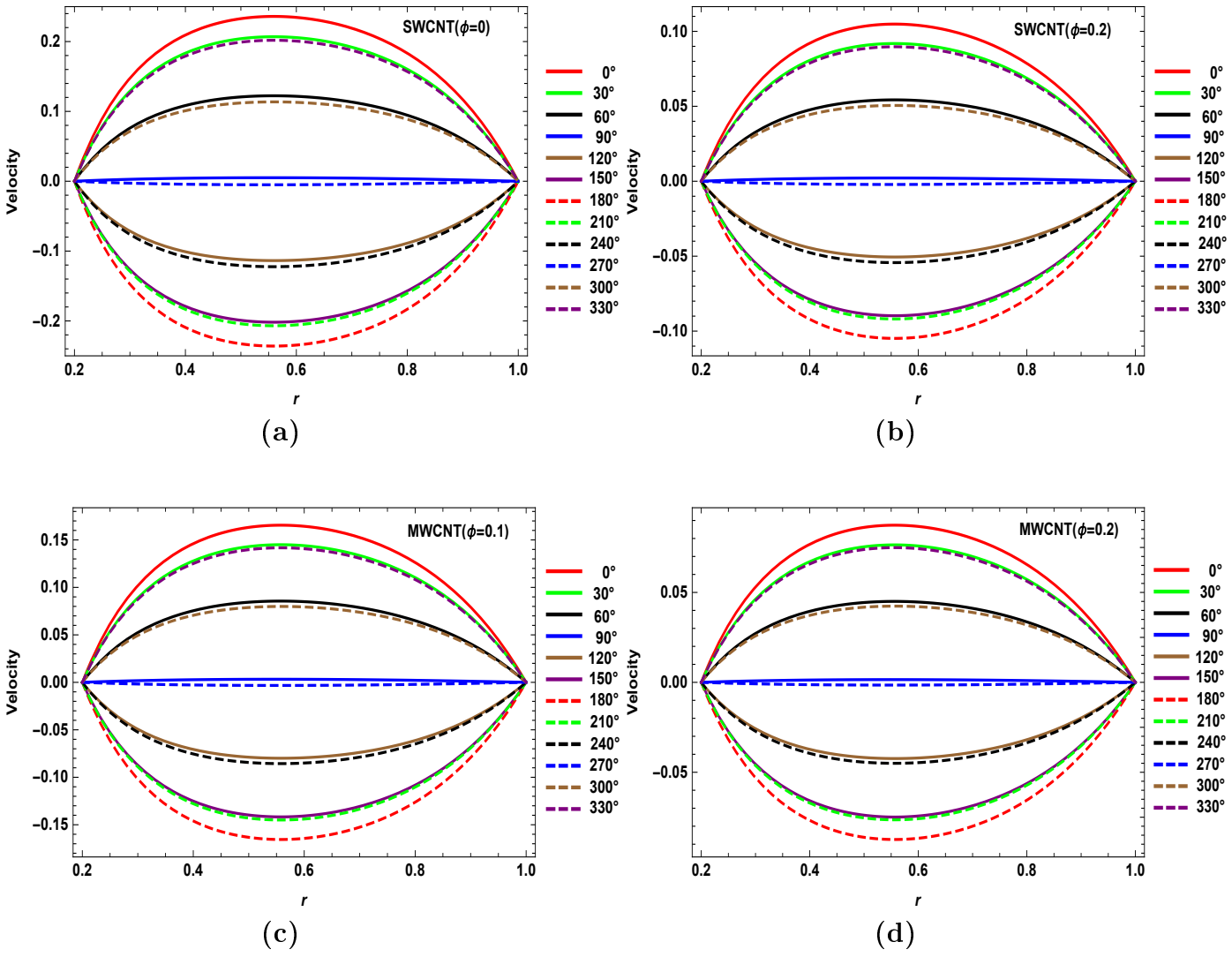

Figure 4.1: Variation of velocity distribution **(a)** Base fluid ($\phi = 0$); **(b)** SWCNT ($\phi = 0.2$); **(c)** MWCNT ($\phi = 0.1$) and **(d)** MWCNT ($\phi = 0.2$); when $M = 5$, $D_a = 0.1$, $Re_\omega = 1$.

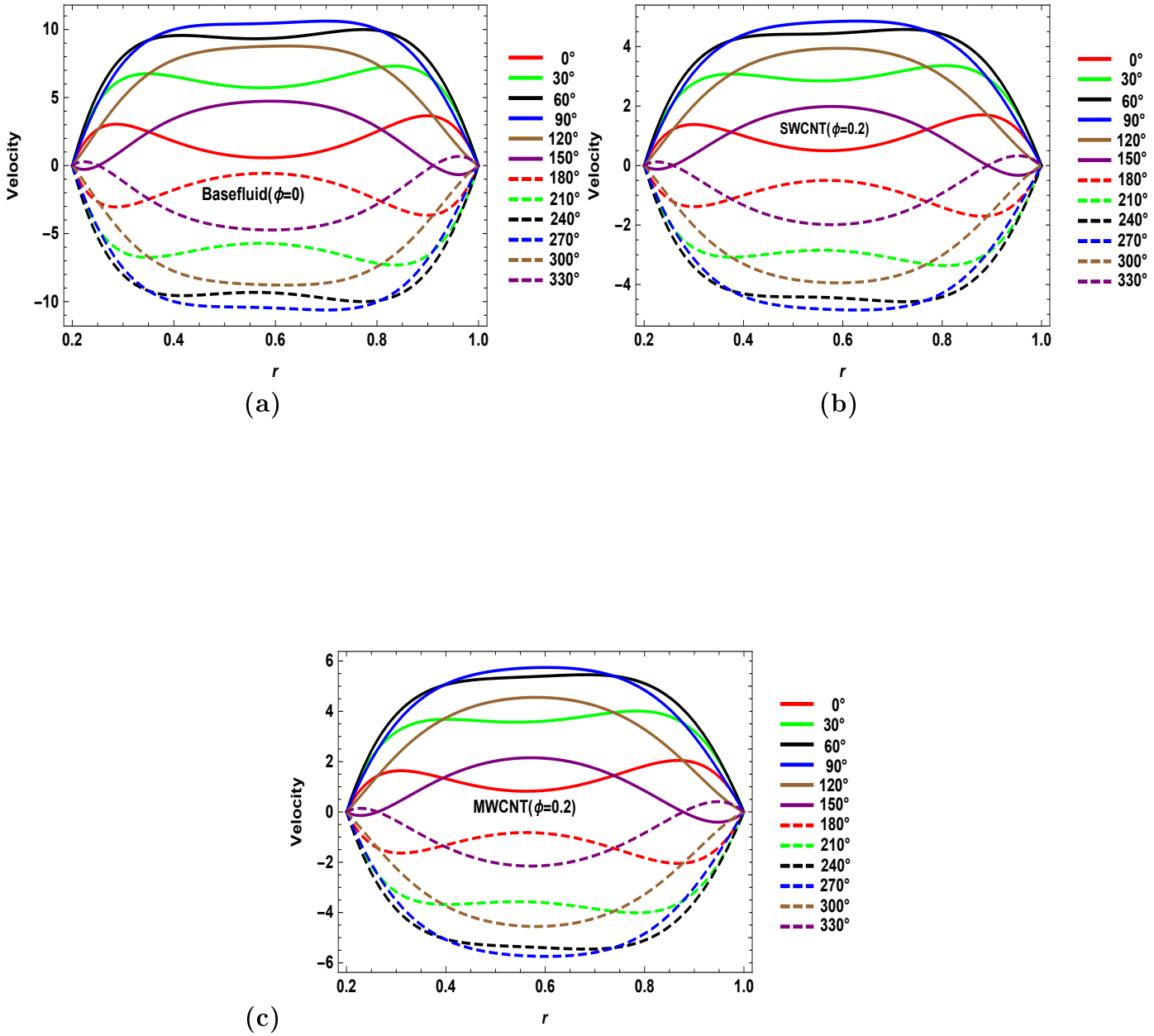

Figure 4.2: Variation of velocity distribution **(a)** Base fluid ($\phi = 0$); **(b)** SWCNT ($\phi = 0.2$) and **(c)** MWCNT ($\phi = 0.2$); when $M = 0$, $D_a = 0.1$, $Re_\omega = 150$.

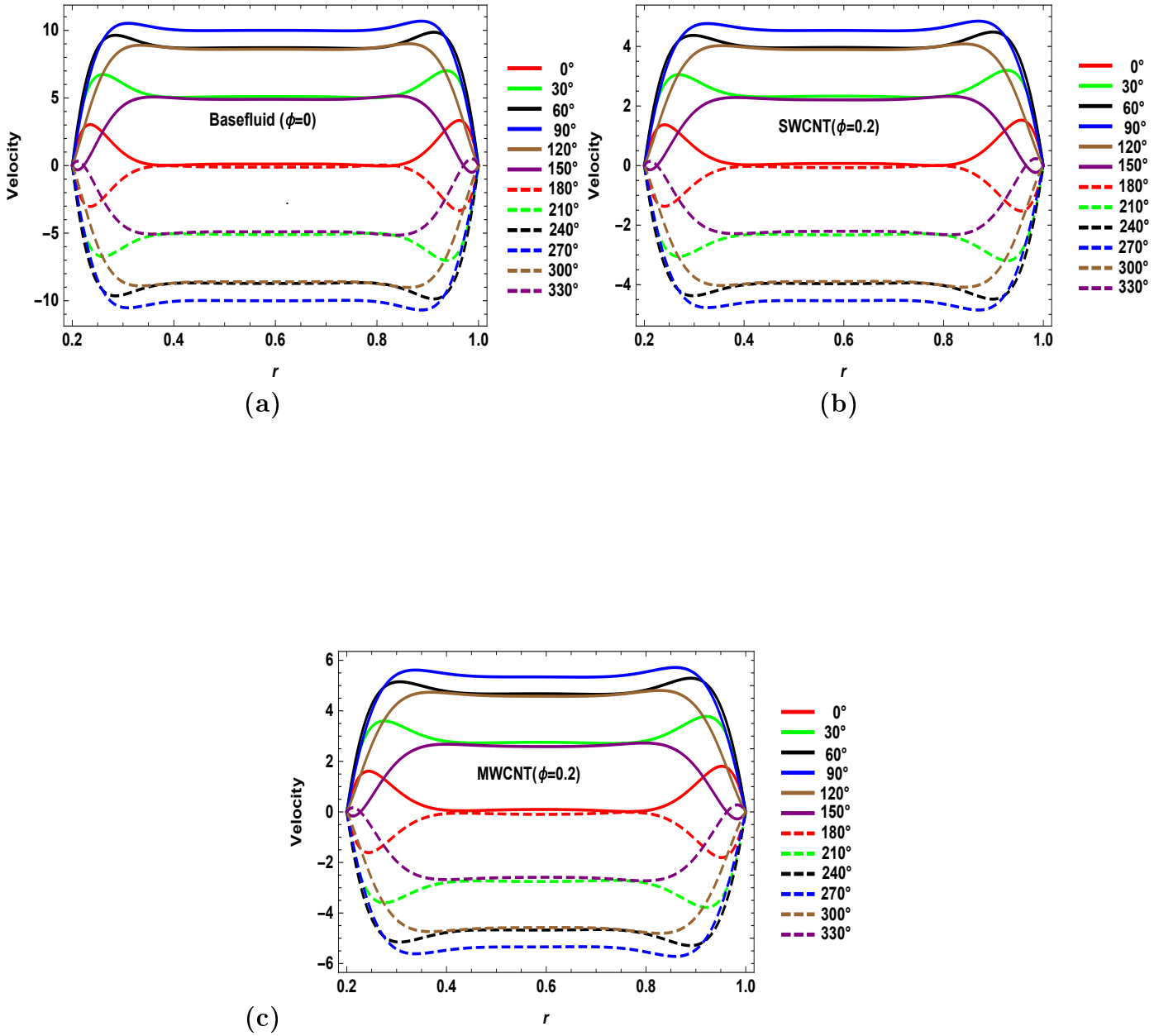

Figure 4.3: Variation of velocity distribution **(a)** Base fluid ($\phi = 0$); **(b)** SWCNT($\phi = 0.2$) and **(c)** MWCNT ($\phi = 0.2$); when $M = 0$, $D_a = 0.1$, $Re_\omega = 900$.

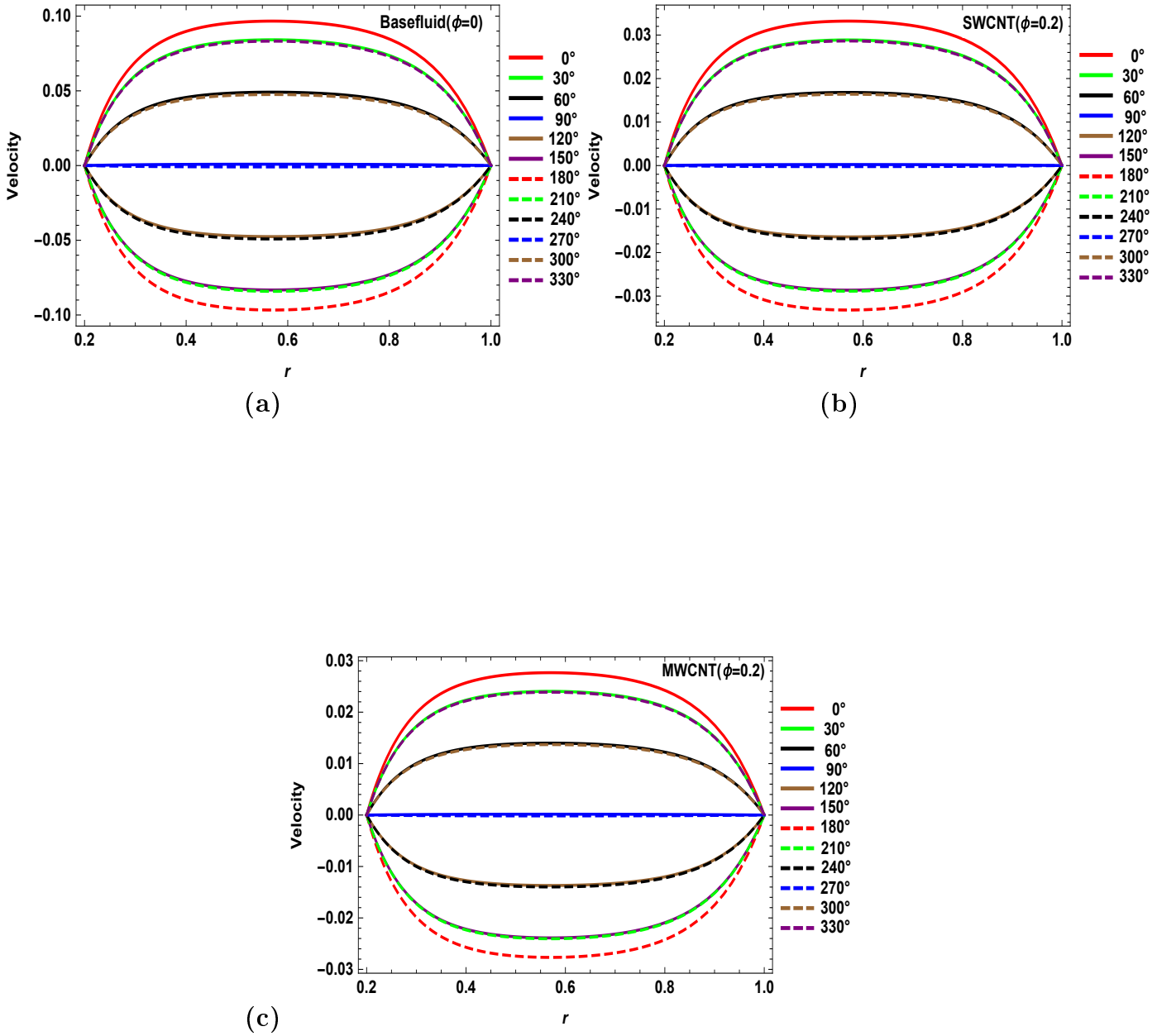

Figure 4.4: Variation of velocity distribution **(a)** Base fluid ($\phi = 0$); **(b)** SWCNT ($\phi = 0.2$) and **(c)** MWCNT ($\phi = 0.2$); when $M = 10$, $D_a = 0.1$, $Re_\omega = 1$.

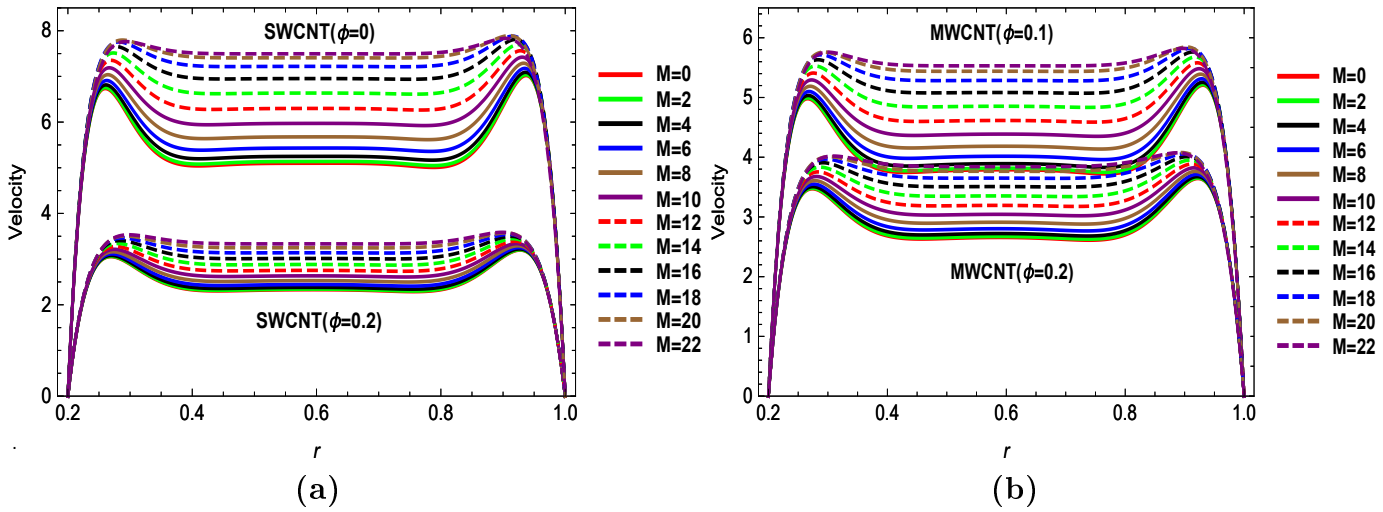

Figure 4.5: Variation of velocity distribution for various values of M **(a)** SWCNT ($\phi = 0$) and ($\phi = 0.2$); **(b)** MWCNT ($\phi = 0.1$) and ($\phi = 0.2$); when $D_a = 0.1$, $Re_\omega = 900$, $t = 30$.

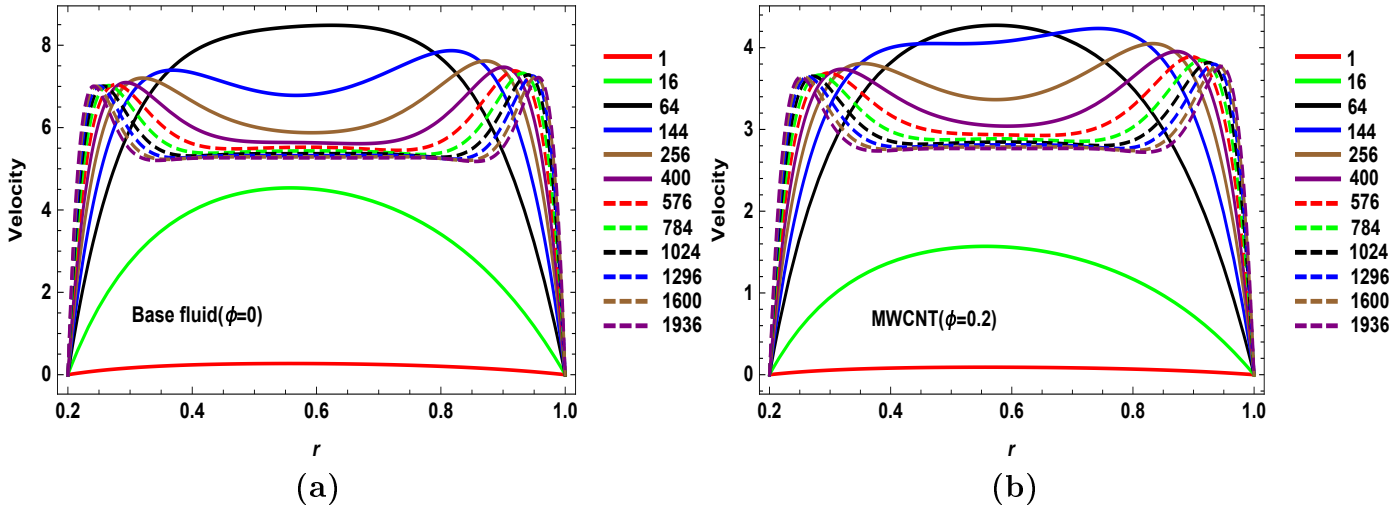

Figure 4.6: Variation of velocity distribution for different values of Re_ω **(a)** Base fluid ($\phi = 0$); **(b)** MWCNT ($\phi = 0.2$); when $M = 5$, $D_a = 0.1$, $t = 30$.

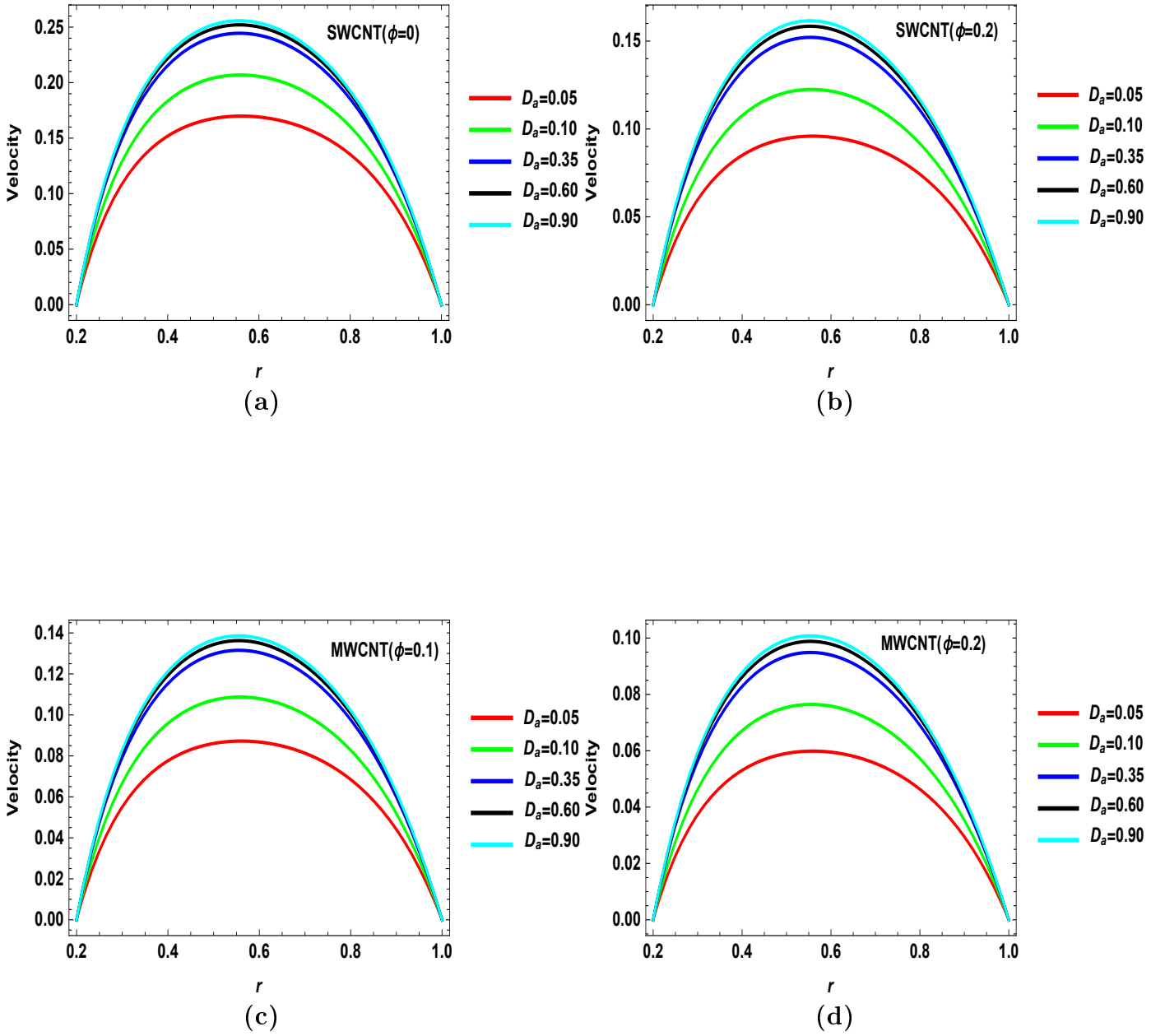

Figure 4.7: Variation of velocity distribution for different values of D_a **(a)** SWCNT ($\phi = 0$); **(b)** SWCNT ($\phi = 0.2$); **(c)** MWCNT ($\phi = 0.1$) and **(d)** MWCNT ($\phi = 0.2$); when $M = 5$, $t = 30$, $Re_\omega = 1$.

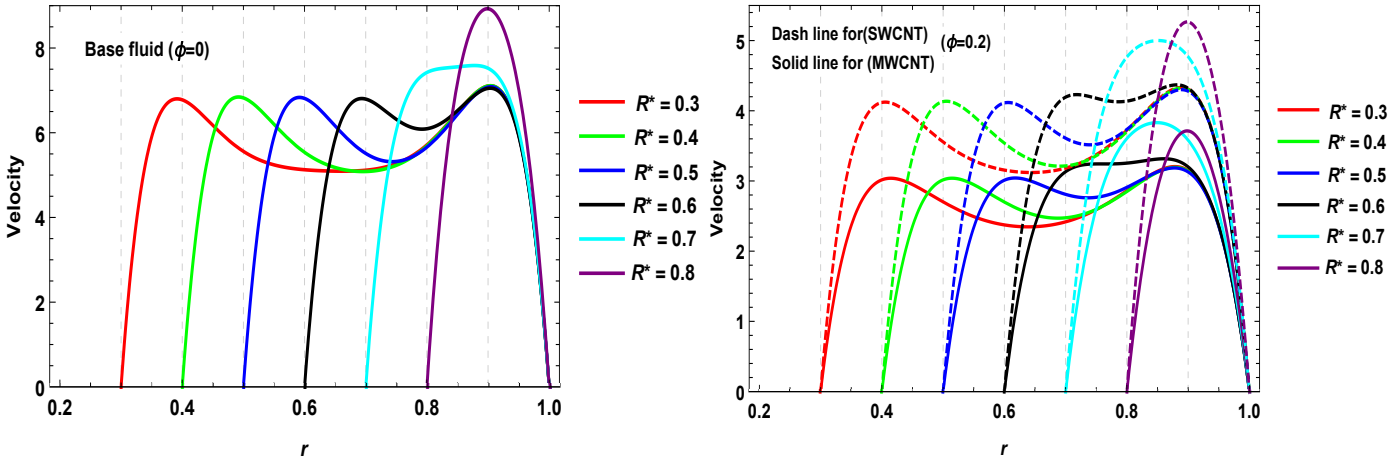

(a) (b)

Figure 4.8: Variation of velocity distribution for different values of R^* **(a)** Base fluid ($\phi = 0$); **(b)** SWCNT and MWCNT ($\phi = 0.2$); when $t = 30$, $D_a = 0.1$, $Re_\omega = 400$, $M = 0$.

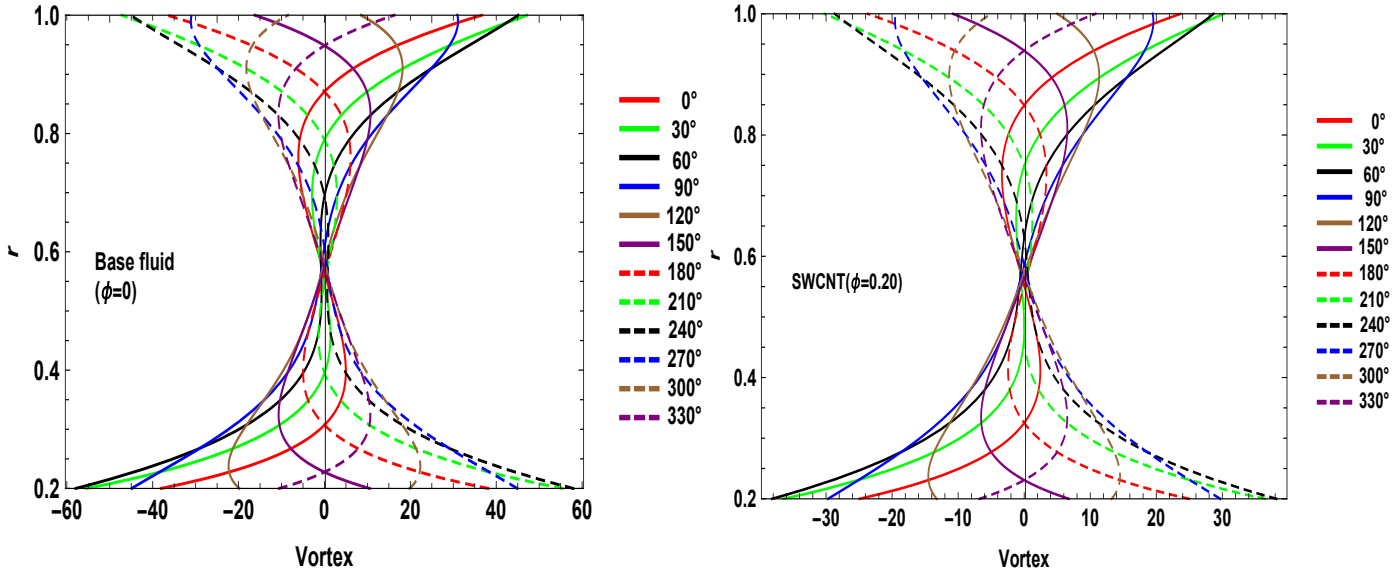

(a) (b)

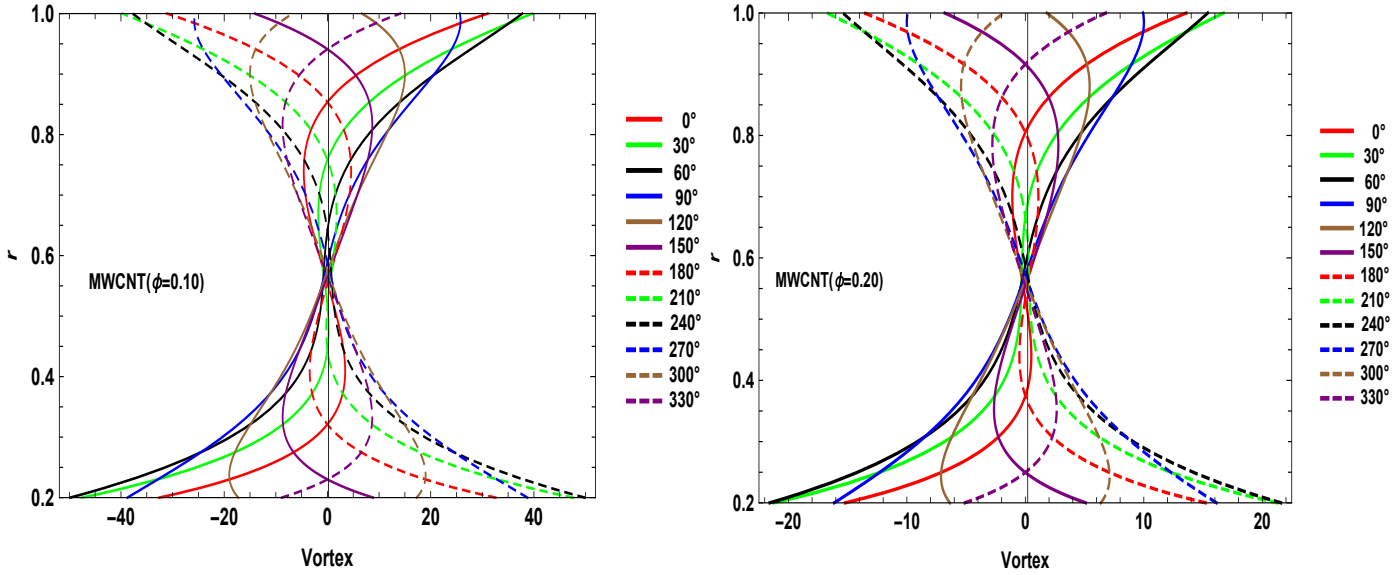

(c) (d)

Figure 4.9: Variation of vortex profile t for **(a)** Base fluid ($\phi = 0$); **(b)** SWCNT ($\phi = 0.2$); **(c)** MWCNT ($\phi = 0.10$) and **(d)** MWCNT ($\phi = 0.2$); when $Re_\omega = 100$, $M = 5$ and $D_a = 0.1$

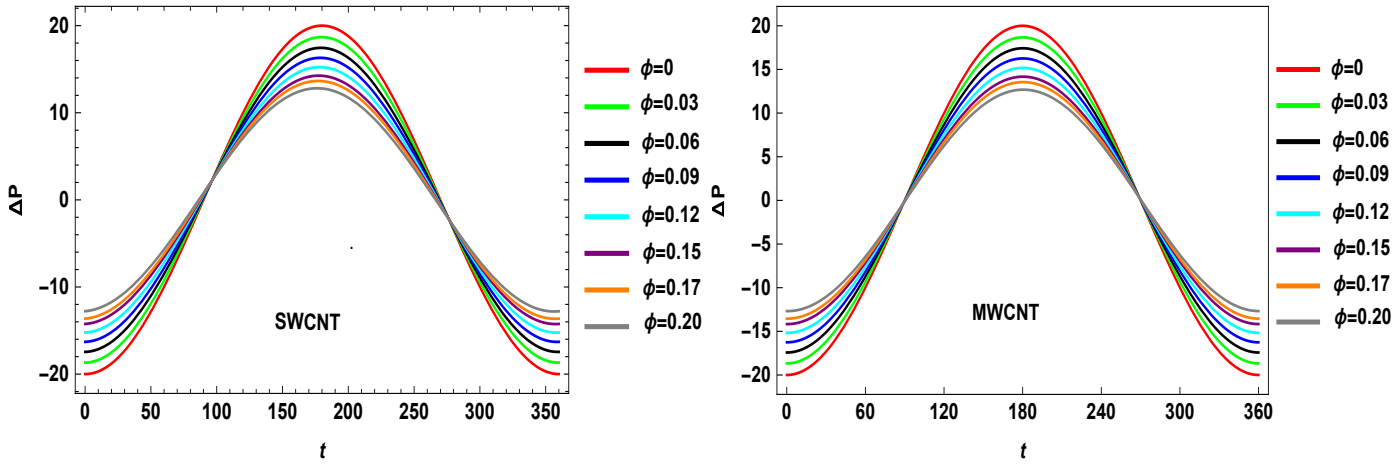

(a) (b)

Figure 4.10: Pressure gradient for **(a)** SWCNT and **(b)** MWCNT; when $M = 10$, $D_a = 0.1$, $Re_\omega = 10$, $A = 20$ and $R^* = 0.2$..

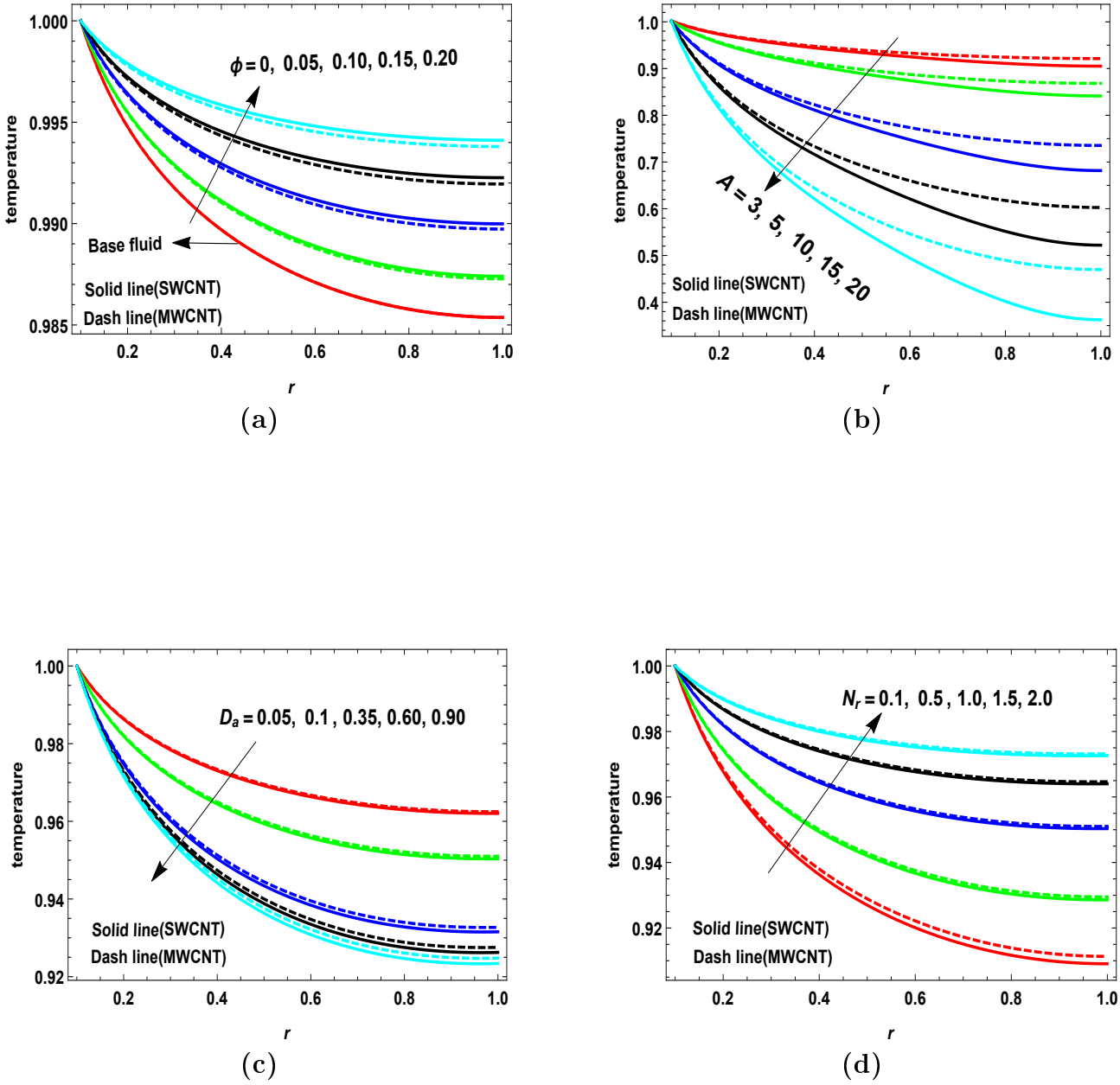

Figure 4.11: Temperature distribution for SWCNTs and MWCNTs (a) Effect of ϕ when $Re_\omega = 1, D_a = 0.1, M = 10, N_r = 2$;(b) Effect of A when $Re_\omega = 20, D_a = 0.1, M = 20, N_r = 2$;(c) Effect of D_a when $Re_\omega = 1, M = 0, N_r = 1$;(d) Effect of N_r when $Re_\omega = 1, D_a = 0.1, M = 0$;

Chapter 5

Conclusion

In this thesis we studied the Magnetohydrodynamics pulsatile flow of electrically conducting nanofluid between two concentric cylinder under the impact of a thermal radiation via porous material. The governing partial differential equations were first transformed to ordinary differential equations. The new system was then solved in terms of modified Bessel functions of first and second kind with the help MATHEMATICA. A analytical solution for velocity distribution, temperature distribution, and pressure gradient and results are displayed in the form of graphs. We can draw the following results and conclusions from our research:

- The maximum amplitude of velocity decreases by increasing the CNTs volume fraction ϕ while an opposite behavior is observed by increasing the Darcy parameter.
- By increasing the Womersley numbers velocity shows increasing behavior close to the cylinder wall but at mean position and for low values of Womersley numbers velocity behaviour rapidly increase. While it is stable for larger values of Womersley number.
- By increasing the pressure gradient amplitude and Darcy parameter, the temperature decreases while it increases with the increase in thermal radiation parameter.

- The inclusion of carbon nanoparticles raises the temperature of ordinary fluid significantly. Nanofluids are good coolants compared to natural base fluids since they are enabled to get control of more warmth than average base fluids.
- Temperature profile is significantly affected due to presence of SWCNTs and MWCNTs.

Bibliography

[1] E.G. Richardson and E. Tyler. The transverse velocity gradient near the mouths of pipes in which an alternating or continuous flow of air is established. *Proceedings of the Physical Society*, **42**:1–15, 1929.

[2] J.R. Womersley. Oscillatory motion of a viscous liquid in a thin-walled elastic tube—i: The linear approximation for long waves. *The London, Edinburgh, and Dublin Philosophical Magazine and Journal of Science*, **46**:199–221, 1955.

[3] S. Uchida. The pulsating viscous flow superposed on the steady laminar motion of incompressible fluid in a circular pipe. *Zeitschrift für angewandte Mathematik und Physik ZAMP*, **7**:403–422, 1956.

[4] H.B. Atabek and C.C. Chang. Oscillatory flow near the entry of a circular tube. *Zeitschrift für angewandte Mathematik und Physik ZAMP*, **12**:185–201, 1961.

[5] S. Kakac and Y. Yener. Exact solution of the transient forced convection energy equation for timewise variation of inlet temperature. *International Journal of Heat and Mass Transfer*, **16**:2205–2214, 1973.

[6] V.K. Stud, G.S. Sekhon, and R.K. Mishra. Pumping action on blood by a magnetic field. *Bulletin of mathematical biology*, **39**:385–390, 1977.

[7] J. Sucec. An improved quasi-steady approach for transient conjugated forced convection problems. *International Journal of Heat and Mass Transfer*, **24**:1711–1722, 1981.

[8] H.L. Agrawal and B. Anwarudin. Peristaltic flow of blood in a branch. *Ranchi Univ. Math. J*, **15**:111–121, 1984.

[9] P. Chaturani and V. Palanisamy. Pulsatile flow of blood with periodic body acceleration. *International Journal of Engineering Science*, **29**:113–121, 1991.

[10] J. Madjalani and H.A. Chibli. Pulsatory channel flows with arbitrary pressure gradients. In *3rd Theoretical Fluid Mechanics Meeting*, pages 24–26, 2002.

[11] M. El-Shahed. Pulsatile flow of blood through a stenosed porous medium under periodic body acceleration. *Applied Mathematics and Computation*, **138**:479–488, 2003.

[12] A. Yakhot and L. Grinberg. Phase shift ellipses for pulsating flows. *Physics of Fluids*, **15**:2081–2083, 2003.

[13] I.M. Eldesoky and A.A. Mousa. Peristaltic flow of a compressible non-newtonian maxwellian fluid through porous medium in a tube. *International Journal of Biomathematics*, **3**:255–275, 2010.

[14] A.A.A. Hassan and A.A.E. Mohammed. Effect of couple stresses on a pulsatile mhd biviscosity fluid flow with heat and mass transfer through a non-darcy porous medium between two permeable parallel plates. *Journal of Porous Media*, **14**:253–264.

[15] J. Majdalani. Exact navier-stokes solution for the pulsatory viscous channel flow with arbitrary pressure gradient. *Journal of propulsion and power*, **24**:1412–1423, 2008.

[16] S.U.S. Choi, Z.G. Zhang, W. Yu, and F.E. Lockwood. Anomalous thermal conductivity enhancement in nanotube suspensions. *Applied physics letters*, **79**:2252–2254, 2001.

[17] M.S. Liu, M.C.C. Lin, I.T. Huang, and C.C. Wang. Enhancement of thermal conductivity with carbon nanotube for nanofluids. *International communications in heat and mass transfer*, **32**:1202–1210, 2005.

[18] W. Yu, D.M. France, J.L. Routbort, and S.U.S. Choi. Review and comparison of nanofluid thermal conductivity and heat transfer enhancements. *Heat transfer engineering*, **29**:432–460, 2008.

[19] S.U.S. Choi. Nanofluids: from vision to reality through research. *Journal of Heat transfer*, **131**:1–9, 2009.

[20] J. Buongiorno. Convective transport in nanofluids. **128**:240–250, 2006.

[21] N.S. Akbar and S. Nadeem. Mixed convective magnetohydrodynamic peristaltic flow of a jeffrey nanofluid with newtonian heating. *Zeitschrift für Naturforschung A*, **68**:433–441, 2013.

[22] A.M. Rashad, S. Abbasbandy, and A.J. Chamkha. Non-darcy natural convection from a vertical cylinder embedded in a thermally stratified and nanofluid-saturated porous media. *Journal of heat transfer*, **136**:1–9, 2014.

[23] F. Shahzad, Haq R.U., and Q.M. Al-Mdallal. Water driven cu nanoparticles between two concentric ducts with oscillatory pressure gradient. *Journal of Molecular Liquids*, **224**:322–332, 2016.

[24] S.M. Rassoulinejad-Mousavi and H. Yaghoobi. Effect of non-linear drag term on viscous dissipation in a fluid saturated porous medium channel with various boundary conditions at walls. *Arabian Journal for Science and Engineering*, **39**:1231–1240, 2014.

[25] M. Sheikholeslami, Mustafa M.T., and D.D. Ganji. Nanofluid flow and heat transfer over a stretching porous cylinder considering thermal radiation. *Iranian Journal of Science and Technology (Sciences)*, **39**:433–440, 2015.

[26] R.L. Hamilton and O.K. Crosser. Thermal conductivity of heterogeneous two-component systems. *Industrial & Engineering chemistry fundamentals*, **1**:187–191, 1962.

[27] S. Iijima. Helical microtubules of graphitic carbon. *nature*, **354**:56–58, 1991.

[28] R. Ramasubramaniam, J. Chen, and H. Liu. Homogeneous carbon nanotube/polymer composites for electrical applications. *Applied Physics Letters*, **83**:2928–2930, 2003.

[29] Q.Z. Xue. Model for thermal conductivity of carbon nanotube-based composites. *Physica B: Condensed Matter*, **368**:302–307, 2005.

[30] Y. Ding, H. Alias, D. Wen, and R.A. Williams. Heat transfer of aqueous suspensions of carbon nanotubes (cnt nanofluids). *International Journal of Heat and Mass Transfer*, **49**:240–250, 2006.

[31] R. Kamali and A.R. Binesh. Numerical investigation of heat transfer enhancement using carbon nanotube-based non-newtonian nanofluids. *International Communications in Heat and Mass Transfer*, **37**:1153–1157, 2010.

[32] J. Wang, J. Zhu, X. Zhang, and Y. Chen. Heat transfer and pressure drop of nanofluids containing carbon nanotubes in laminar flows. *Experimental Thermal and Fluid Science*, **44**:716–721, 2013.

[33] T. Hayat, F. Haider, T. Muhammad, and A. Alsaedi. Three-dimensional rotating flow of carbon nanotubes with darcy-forchheimer porous medium. *PLoS One*, **12**:e0179576, 2017.

[34] L.I. Manevitch, V.V. Smirnov, M. Strozzi, and F. Pellicano. Nonlinear optical vibrations of single-walled carbon nanotubes. *International Journal of Non-Linear Mechanics*, **94**:351–361, 2017.

[35] B. Mahanthesh, B.J. Gireesha, N.S. Shashikumar, and S.A. Shehzad. Marangoni convective mhd flow of swcnt and mwcnt nanoliquids due to a disk with solar

radiation and irregular heat source. *Physica E: Low-dimensional Systems and Nanostructures*, **94**:25–30, 2017.

[36] S. Nadeem and I. Shahzadi. Single wall carbon nanotube (swcnt) analysis on peristaltic flow in an inclined tube with permeable walls. *International Journal of Heat and Mass Transfer*, **97**:794–802, 2016.

[37] R.U. Haq, F. Shahzad, and Q.M. Al-Mdallal. Mhd pulsatile flow of engine oil based carbon nanotubes between two concentric cylinders. *Results in Physics*, **7**:57–68, 2017.

[38] M. Hamid, Z.H. Khan, W.A. Khan, and R.U. Haq. Natural convection of water-based carbon nanotubes in a partially heated rectangular fin-shaped cavity with an inner cylindrical obstacle. *Physics of Fluids*, **31**:103607, 2019.

[39] Y. Xiao, N.A. Shah, and T. Irshad. Magneto-hydrodynamics natural convection flows of viscous carbon nanotubes nanofluids with generalized fourier's law in a vertical cylinder. *Mathematical Methods in the Applied Sciences*, 2020.

[40] O. Cicek, A.F. Baytas, and A.C. Baytas. Entropy generation of mixed convection of swcnt–water nanofluid filled an annulus with a rotating cylinder and porous lining under ltne. *International Journal of Numerical Methods for Heat & Fluid Flow*, 2020.

[41] A. Bhattacharyya, G.S. Seth, R. Kumar, and A.J. Chamkha. Simulation of cattaneo–christov heat flux on the flow of single and multi-walled carbon nanotubes between two stretchable coaxial rotating disks. *Journal of Thermal Analysis and Calorimetry*, **139**:1655–1670, 2020.

[42] M. Ramzan, M. Sheikholeslami, J.D. Chung, and A. Shafee. Melting heat transfer and entropy optimization owing to carbon nanotubes suspended casson nanoliquid flow past a swirling cylinder-a numerical treatment. *AIP Advances*, **8**:115130, 2018.

[43] A. Sofiyev, R.P.O. Bayramov, and S.H.O. Heydarov. The forced vibration of infinitely long cylinders reinforced by carbon nanotubes subjected to combined

internal and ring-shaped compressive pressures. *Mathematical Methods in the Applied Sciences*, 2020.

[44] H.C. Brinkman. The viscosity of concentrated suspensions and solutions. *The Journal of Chemical Physics*, **20**:571–571, 1952.

[45] K. Khanafer, K. Vafai, and M. Lightstone. Buoyancy-driven heat transfer enhancement in a two-dimensional enclosure utilizing nanofluids. *International journal of heat and mass transfer*, **46**:3639–3653, 2003.